Short article

Developmental Cell

# Genetic perturbation of AMP biosynthesis extends lifespan and restores metabolic health in a naturally short-lived vertebrate

## Graphical abstract

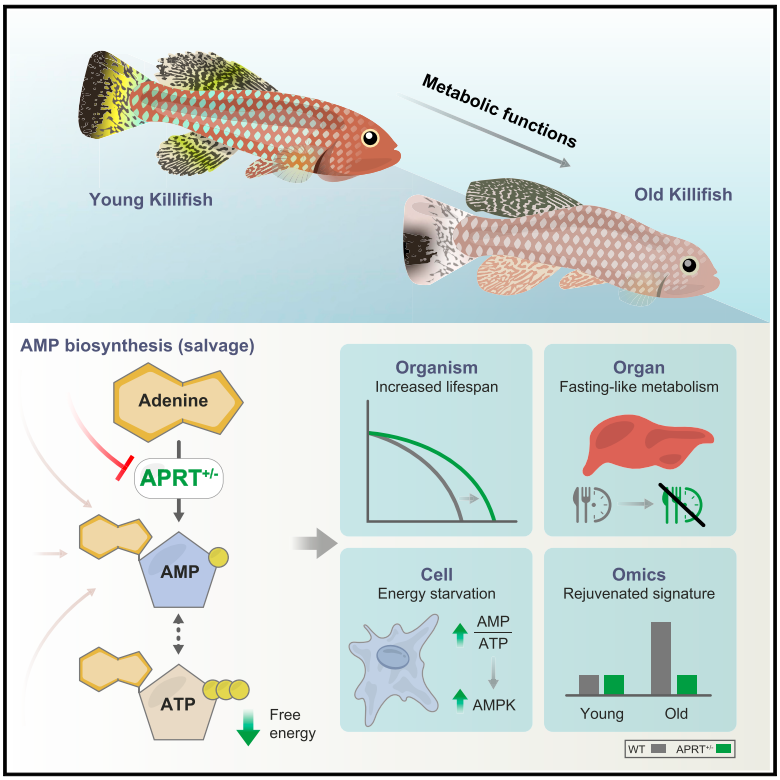


## Highlights

- Reduction of APRT expression in the turquoise killifish promotes longevity
- APRT heterozygous fish exhibit rejuvenation of metabolic functions during aging
- Cellular phenotypes include a fasting-like metabolic switch and AMPK activation
- Lifelong intermittent fasting abolishes the longevity benefits

## Authors

Gwendoline Astre, Tehila Atlan, Uri Goshtchevsky, ..., Tomer Levy, Erez Y. Levanon, Itamar Harel

## Correspondence

itamarh@mail.huji.ac.il

## In brief

Astre and Atlan et al. use the turquoise killifish to genetically restore the energy balance that declines in old age and underlies various age-related pathologies. By targeting the biosynthesis of AMP, the precursor for ATP, they rejuvenate fish metabolism and promote longevity, and this presents a promising mechanism to enhance metabolic health.

Astre et al., 2023, Developmental Cell *58*, 1350–1364
August 7, 2023 
https://doi.org/10.1016/j.devcel.2023.05.015

CellPress

CellPress

Developmental Cell

Short article

# Genetic perturbation of AMP biosynthesis extends lifespan and restores metabolic health in a naturally short-lived vertebrate

Gwendoline Astre,[1,6] Tehila Atlan,[1,6] Uri Goshtchevsky,[1] Adi Oron-Gottesman,[1] Margarita Smirnov,[2] Kobi Shapira,[3] Ariel Velan,[1] Joris Deelen,[4,5] Tomer Levy,[1] Erez Y. Levanon,[3] and Itamar Harel[1,7,*]

[1]Department of Genetics, the Silberman Institute, the Hebrew University of Jerusalem, Givat Ram, Jerusalem 91904, Israel

[2]Central Fish Health Laboratory, Department of Fisheries and Aquaculture, Ministry of Agriculture and Rural Development, Nir David 10803, Israel

[3]Mina and Everard Goodman Faculty of Life Sciences, Bar-Ilan University, Ramat-Gan 52900, Israel

[4]Max Planck Institute for Biology of Ageing, Cologne 50931, Germany

[5]Cologne Excellence Cluster on Cellular Stress Responses in Ageing-Associated Diseases (CECAD), University of Cologne, Cologne 50931, Germany

[6]These authors contributed equally

[7]Lead contact

*Correspondence: itamarh@mail.huji.ac.il

https://doi.org/10.1016/j.devcel.2023.05.015

## SUMMARY

During aging, the loss of metabolic homeostasis drives a myriad of pathologies. A central regulator of cellular energy, the AMP-activated protein kinase (AMPK), orchestrates organismal metabolism. However, direct genetic manipulations of the AMPK complex in mice have, so far, produced detrimental phenotypes. Here, as an alternative approach, we alter energy homeostasis by manipulating the upstream nucleotide pool. Using the turquoise killifish, we mutate APRT, a key enzyme in AMP biosynthesis, and extend the lifespan of heterozygous males. Next, we apply an integrated omics approach to show that metabolic functions are rejuvenated in old mutants, which also display a fasting-like metabolic profile and resistance to high-fat diet. At the cellular level, heterozygous cells exhibit enhanced nutrient sensitivity, reduced ATP levels, and AMPK activation. Finally, lifelong intermittent fasting abolishes the longevity benefits. Our findings suggest that perturbing AMP biosynthesis may modulate vertebrate lifespan and propose APRT as a promising target for promoting metabolic health.

## INTRODUCTION

Aging is associated with metabolic changes, which in turn, contribute to the onset of age-related diseases.[1–4] A common theme among lifespan regulators is their tight connection to metabolism and energy homeostasis.[5] Thus, extensive efforts have been invested in exploring pro-longevity interventions by targeting primary metabolic pathways.[6] Dietary manipulation, such as dietary restriction and fasting, have emerged as evolutionary-conserved longevity interventions.[4,7] However, the fasting response and its consequences on promoting health and longevity[8–11] are differently regulated between males and females.[12–14] Therefore, a better understanding of the underlying molecular mechanisms is required to design future interventions that target sex-dimorphic age-related diseases.[15–17]

AMP-activated protein kinase (AMPK) is an evolutionary-conserved sensor of cellular energy. Accordingly, AMPK is involved in many physiological responses, including fasting and physical exercise.[5,6] Molecularly, AMPK is activated in response to low energy levels, which are reflected by a higher AMP:ATP ratio in the cell. This activation then restores the cellular energy balance by inhibiting ATP-consuming processes and activating ATP-generating processes,[18,19] including protein metabolism, lipid metabolism, glucose metabolism, and autophagy and mitochondrial homeostasis.[20]

The liver, a central metabolic organ, has an important role in maintaining blood glucose levels and regulating whole-body energy metabolism.[21] Consequently, as a hub for coordinating fasting-feeding transitions,[22] the liver shifts into an energy production mode during fasting, and similar to AMPK activation, the liver uses free fatty acids (FFAs) as an energy source. However, in contrast to AMPK activation, the liver generates glucose for peripheral tissues during fasting (particularly the brain) by activating gluconeogenesis.[23] Thus, although fasting activates AMPK,[20] several differences are also expected between the liver and peripheral tissues (such as the muscle).

So far, the genetic regulation of vertebrate aging by AMPK has been poorly understood.[5,6,24] Although promising findings exist

 

in invertebrate models[25–31] and human genomic studies,[32] genetic mouse models have been so far challenging. Specifically, recent attempts to directly manipulate the AMPK complex in mice display conflicting and adverse phenotypes,[18,33–36] possibly due to the intricate and tissue-specific composition of individual AMPK subunits. Thus, alternative strategies are required.

To address these challenges, we use the turquoise killifish (*Nothobranchius furzeri*), a naturally short-lived fish that undergoes typical vertebrate aging.[37] These fish have recently emerged as an exciting experimental model,[38–43] owing to the availability of advanced genomic and genome editing tools. However, so far, a long-lived genetic killifish model has not been generated. Here, as an indirect approach to alter energy homeostasis, we manipulate the upstream nucleotide pool by mutating adenine phosphoribosyltransferase (APRT). APRT is a key enzyme in the biosynthesis of AMP via the salvage pathway.

Interestingly, *APRT* heterozygous fish display lifespan extension in a male-specific manner, confirming the feasibility of our approach. To explore the underlying mechanism, we use a comprehensive set of *in-vivo* and *in-vitro* approaches and take advantage of the sex-specific effect. Mechanistically, we show that the ability to quickly adapt to nutrient levels was restored in old heterozygous males. These findings further suggest a genetically induced fasting-like response, which correlates with increased cellular AMP:ATP ratios and AMPK activation. Accordingly, intermittent fasting eliminated the longevity benefits. Our findings highlight the potential of the killifish experimental platform and suggest that AMP biosynthesis may be a modulator of vertebrate aging.

## RESULTS

### Targeting AMP biosynthesis by generating a genetic model for APRT

To genetically alter energy homeostasis, we mutated APRT, which irreversibly catalyzes the formation of AMP from adenine and 5-phosphoribosyl-1-pyrophosphate (PRPP) (Figure 1A). We used our recent CRISPR protocols[44–47] to generate an 8 base-pair deletion allele (Δ8) in the killifish *APRT* gene, which is predicted to produce a frameshift and a loss of function (Figure 1B). We then outcrossed this line (for more than 6 generations) to reduce the effect of potential off-target mutations. Mating heterozygous $APRT^{\Delta 8/+}$ pairs follow the expected Mendelian ratios with respect to the genotypes of the fertilized eggs ($p = 0.9$, $\chi^2$ test, Figure S1A). Heterozygous fish displayed no significant difference in fecundity (Figure S1B) or in the highly uniform egg size (Figure S1C). A modest growth effect was observed, specifically in adult males (Figures S1D and S1E). After hatching, we failed to detect any adult $APRT^{\Delta 8/\Delta 8}$ fish, suggesting that the homozygous mutation is embryonic lethal ($p = 0.0006$, $\chi^2$ test, Figure S1A).

### Male-specific lifespan extension in $APRT^{\Delta 8/+}$ heterozygous fish

In view of the central role of AMP biosynthesis in energy homeostasis, we were curious to examine the effect on lifespan. Surprisingly, the lifespan of $APRT^{\Delta 8/+}$ heterozygous males was significantly longer (~17% increase in median lifespan, log-rank test, $p = 0.021$, Figure 1C), whereas female lifespan was not affected (log rank test, $p = 0.86$, Figure 1D). Similar results are also observed in regard to maximal lifespan[48] (~24% increase, 90$^{th}$ percentile, Table S1). Histological evaluation suggested that gross age-related pathologies were not dramatically altered in heterozygous fish (Figures S1F and S1G; Table S1), and in agreement with previous reports,[41] the lifespan of wild-type (WT) males and females were comparable (Figure 1E). Taken together, our findings highlight the role of AMP biosynthesis in modulating lifespan. Furthermore, our phenotype was observed primarily in males, thus providing an opportunity to compare the differential effects on males and females.[17,49,50]

### The $APRT^{\Delta 8/+}$ mutation produces a distinct transcriptional response in male livers

To first explore the effect of the $APRT^{\Delta 8/+}$ mutation in males, we compared the transcriptome of the liver from young (6.5 weeks) or old (15 weeks) fish, either WT or $APRT^{\Delta 8/+}$ heterozygous (Figure 1F). Principle component analysis (PCA) demonstrated that in some cases, old $APRT^{\Delta 8/+}$ fish segregates with young samples (PC1, Figure S1H). As expected, the expression level of *APRT* transcripts was reduced by ~50% in heterozygous fish (probably as a result of nonsense-mediated mRNA decay of the CRISPR-edited allele, Figure S1I), suggesting that the $APRT^{\Delta 8}$ is a loss-of-function allele.

The differential expression analysis, which compared WT with $APRT^{\Delta 8/+}$ fish, revealed a total of 1,612 downregulated and 1,816 upregulated genes (FDR of 0.05, Table S2). We next conducted gene set enrichment analysis (GSEA) using gene ontology (GO). Our analysis indicated that many pathways enriched in heterozygous fish overlap with a fasting-like response and a canonical AMPK transcriptional signature.[20] These pathways include increased fatty acid β-oxidation, autophagy, and mitochondrial homeostasis, as well as a reduction in ribosome biogenesis and cell proliferation (Figure 1F, left). Representative driver genes are also indicated (Figure 1F, right). Interestingly, the downregulation in cell proliferation and aging-related pathways in heterozygous fish provides a possible link to the observed smaller size (Figure S1E) and longer lifespans, respectively. Involvement of the AMP/AMPK axis was further suggested by a distinct subunit composition of the AMPK complex in heterozygous fish, specifically upregulating the *PRKAA1* catalytic the *PRKAG1* regulatory subunits (Figure S1J).

To better investigate how carbohydrate metabolism is altered, we used gene set variation analysis (GSVA)[51] and the Reactome Pathway Database.[52] Our data indicated that heterozygous fish undergo a metabolic switch, specifically upregulating gluconeogenesis at the expense of glycolysis (Figure S1K). The expression levels of rate-limiting enzymes are also indicated, including *Hexokinase 1* (*HK1*, for glycolysis) and *Fructose-Bisphosphatase 1* (*FBP1*, for gluconeogenesis). These findings are in agreement with the mammalian fasting response, in which hepatocytes inhibit glycolysis to generate glucose for peripheral tissues.[53,54]

### Comparing the transcriptional signature of the $APRT^{\Delta 8/+}$ mutation with classical longevity interventions in mice

Many genetic, pharmacological, and dietary interventions can extend mammalian lifespan. However, as genetic manipulation of AMP biosynthesis is an unexplored class of longevity

**A** ATP production via the nucleotide salvage pathway

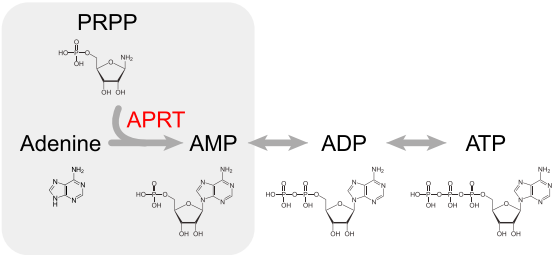


**B** Generation of *APRT* CRISPR mutant

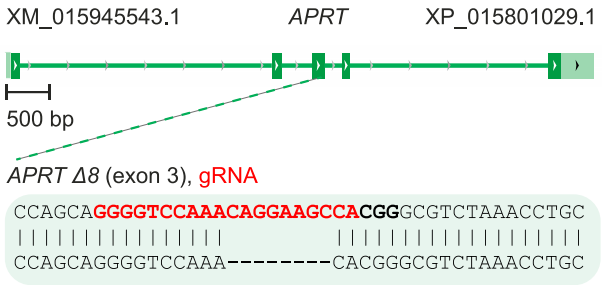


**C** Lifespan of *APRT*$^{\Delta 8/+}$ males

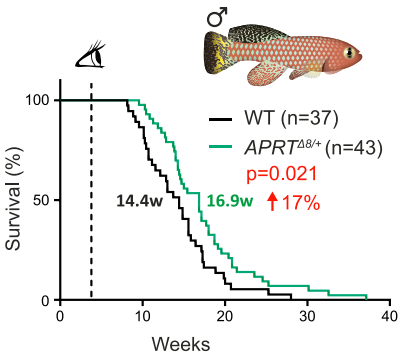


**D** Lifespan of *APRT*$^{\Delta 8/+}$ females

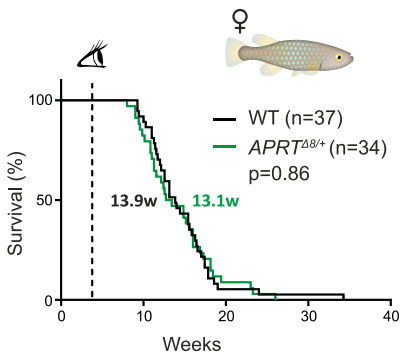


**E** Male and female lifespan

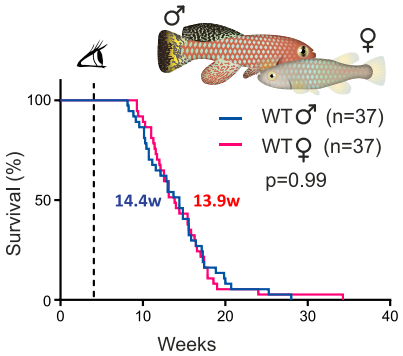


**F** GO analysis comparing hepatic gene expression in WT and *APRT*$^{\Delta 8/+}$ males

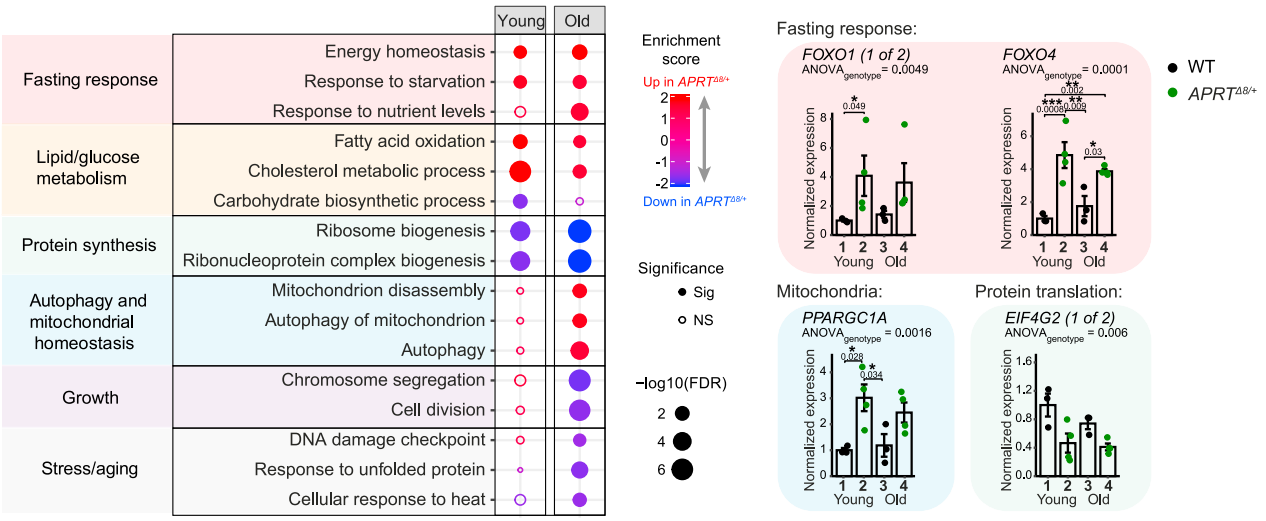


**Figure 1. Male-specific lifespan extension of *APRT*$^{\Delta 8/+}$ fish**

(A) AMP biosynthesis pathway. The adenine phosphoribosyltransferase enzyme (APRT) irreversibly catalyzes adenine and PRPP (5-phosphoribosyl-1-pyrophosphate) into AMP.

(B) Generation of an *APRT* CRISPR mutant with an 8 bp deletion (Δ8). Guide RNA (red) and protospacer adjacent motif (PAM) in bold.

(C–E) Lifespan of WT and *APRT*$^{\Delta 8/+}$ fish for males (C) and females (D). (E) Overlay of the male and female lifespans using data from (C) and (D). Lifespan records were initiated at 4 weeks, "eye" symbol). p values for differential survival in log rank tests, median survival, and cohort size are indicated.

(F) Left: functional enrichments (GO, FDR < 5%) using GSEA for differential gene expression between WT and *APRT*$^{\Delta 8/+}$ male fish, either young (group #1 and 2), or old (group #3 and 4). Right: relative expression (normalized to young WT) of driver genes from the pathways on the left. Each symbol represents an individual fish. Significance was calculated using two-way ANOVA and Tukey post hoc.

intervention in vertebrates, we were curious to explore which molecular pathways overlap between *APRT*$^{\Delta 8/+}$ and other classical interventions. Therefore, we used a comprehensive RNA-sequencing dataset that characterized the hepatic responses to 8 different longevity interventions,[55] including acarbose, 17-α-estradiol, rapamycin, Protandim (a weak Nrf2 activator), caloric restriction (CR, 40%), methionine restriction (0.12%), GHRKO, and Pit1 knockout (Snell dwarf mice). We then performed functional enrichment analysis for differentially expressed genes in heterozygous fish, focusing on pathways that were already enriched in the mouse dataset[55] (Figure 2A; Table S2).

Applying unsupervised clustering assisted us in identifying that *APRT*$^{\Delta 8/+}$ clustered with methionine restriction, 17-α-estradiol, and Protandim (Figure 2A, right). Within this cluster, partial pathway overlaps include response to starvation, reduced oxidative phosphorylation, and downregulation of insulin/IGF1 and mechanistic target of rapamycin (mTOR) pathways (Figure S1E). Upregulated pathways included fatty acid β-oxidation and response to estrogen. Together, our findings provide important insights into possible mechanisms of action that are shared with other longevity interventions, including a fasting-like response, reduced growth factor signaling, and a possible feminizing effect. As the longevity benefit of *APRT*$^{\Delta 8/+}$ was observed primarily in males, we next decided to further narrow down possible regulators by directly comparing males and females.

## Transcriptomic analysis identifies sex- and genotype-specific signatures of aging

To further explore the sex-dimorphic effect of the *APRT*$^{\Delta 8/+}$ mutation, we compared the transcriptome of WT and heterozygous fish, in either males or females. To minimize the effect of feeding cycles, experiments were conducted under metabolic baseline (i.e., 24 h fasting). We performed RNA-sequencing analysis of the liver (Figure 2B). PCA demonstrated that some of the variance is linked to age (PC3, males, Figure S2A). Similar to our previous data (Figure S1I), *APRT* transcript levels were reduced by ~50% in heterozygous fish (Figure S2B).

The differential expression analysis, which compared young and old fish in each experimental condition, revealed a total of 252 downregulated and 193 upregulated genes (FDR of 0.05, Table S2). GSEA and GO analysis confirmed an increase in inflammatory responses as a conserved aging hallmark (Figure 2C).[56,57] As we anticipated that pathways that are modified during aging in male *APRT*$^{\Delta 8/+}$ fish are more likely to contribute to the longevity effect, we focused on male-enriched patterns (Figure 2C, blue shading). These include enrichment for energy production and mitochondrial functions. Representative driver genes are depicted (Figure 2D), including *IGFBP1* (inversely correlated to growth)[58] and *IRS1* (associated with longevity).[5]

## AMP biosynthesis is a sex-dimorphic pathway in killifishes and humans

Performing an age-genotype interaction analysis for males and females suggested additional sex-dimorphic pathways (Table S2). These include the "nucleotide and nucleoside salvage" pathway, which includes AMP salvage and RNA editing (Figure S2C; Tables S2 and S4). We replicated our experimental design in skeletal muscles, another key metabolic organ, which was isolated from the same fish (Figures S2D–S2H). GSEA and GO analysis also confirmed the existence of an inflammatory response as a conserved aging phenotype in muscle and indicated multiple fasting-related pathways that were particularly enriched in males (Figures S2F and S2G). Aging hallmarks display organ-specific temporal signatures.[59] Therefore, in agreement with the distinct metabolic role of the liver, the effect of the *APRT*$^{\Delta 8/+}$ mutation on muscle aging did not fully overlap with the liver (Figures 2C and S2F).

To directly explore basal sex differences in muscle metabolism, we performed an age-sex interaction analysis in WT animals (using GSVA, Figure S2H). Although the expression of *APRT* itself is not sex dimorphic (Figure S2E), sex-specific expression was observed in key metabolic regulators of cellular purine AMP biosynthesis, such as *NT5C2* (*Cytosolic Nucleoside Phosphotransferase 5′N*),[60] as well as autophagy and glycolysis (*Hexokinase-2* or *HK2*, Figure S2H, bottom).[61] These sex-dimorphic pathways are expected to respond differently to alteration in AMP biosynthesis and could mediate the observed phenotypic differences. Interestingly, *Hexokinase* displayed contrasting trends in muscle (*HK2*, Figure S2H) and liver (*HK1*, Figure S1K), further exemplifying the unique role of the liver in glucose metabolism.

To explore the evolutionary conservation of our findings, we analyzed the impact of sex on gene expression across 44 human tissues (The Genotype-Tissue Expression project [GTEx], v8 release).[62] Interestingly, these data show that APRT is a sex-biased gene in 7 of the 44 tested human tissues (local false sign rate [LFSR] $\leq$ 0.05), which was the most significant in the liver (LFSR = 0.00033). Although this study did not explore age-related expression changes, it provides a hint that *APRT* is a sex-dimorphic gene. So far, our RNA-sequencing results suggest that heterozygous males undergo a "metabolic switch." We next set up a series of experiments, focusing on male liver physiology, to explore the functional consequences of this prediction.

## Age-related decline in metabolic plasticity is partially restored in *APRT*$^{\Delta 8/+}$ male livers

The ability of metabolic functions to quickly adapt to nutrient availability declines with age (also known as the "deregulated nutrient sensing" hallmark of aging).[4] We therefore performed a metabolomic analysis by comparing the livers of fully fed fish or animals at metabolic baseline (i.e., fasted, Figure 3A). We characterized polar metabolites (e.g., nucleic acids, sugars), which are typically involved in primary metabolism. This scheme was designed to examine whether metabolic plasticity is indeed deregulated during killifish aging, and if so, to determine the effect of the *APRT*$^{\Delta 8/+}$ mutation. Of a total of 160 unique metabolites, 140 passed our quality control tests (see STAR Methods). Samples seem to segregate according to age (PC2, Figure S3A, left), whereas genotype-related segregation was observed under fasting conditions (PC2, Figure S3A, right). These data confirm the importance of the selected feeding regimens in exposing age- and genotype-specific metabolic signatures.

Focusing on glucose metabolism (Figure S1K), we observed that although glycolytic metabolites (e.g., Fructose 1,6-bisphosphate) were globally high after feeding (groups #1–4), they quickly downregulated during fasting in young fish (groups #5–6). However, many of these metabolites remained at high levels

**A** Pathway enrichment analysis, comparing the transcriptional response of the *APRT*$^{\Delta 8/+}$ mutation (killifish) with common lifespan-extending interventions (mice)

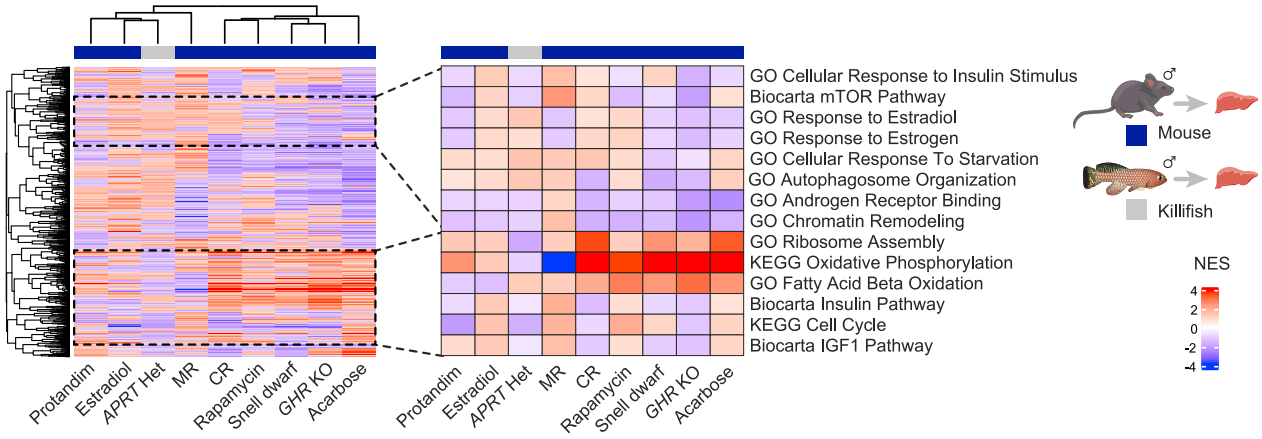


**B** Exploring sex-specific gene expression during liver aging

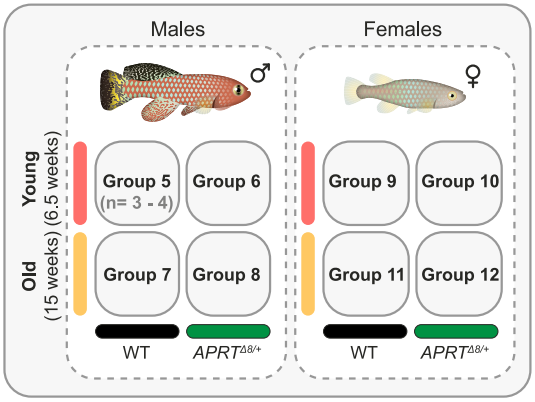


**C** Exploring sex-specific gene expression during liver aging

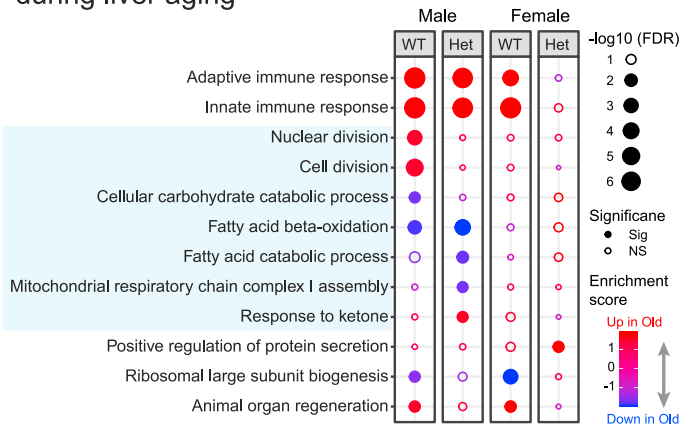


**D** Age- and sex-dependent transcriptional response to the *APRT*$^{\Delta 8/+}$ mutation

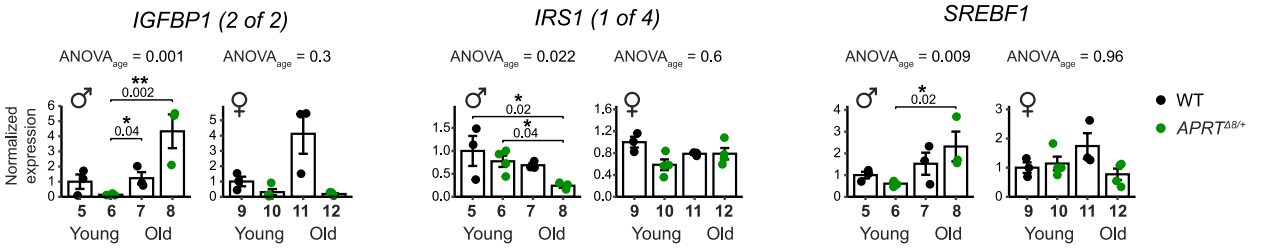


**Figure 2. A distinct transcriptional signature for the *APRT*$^{\Delta 8/+}$ mutation**

(A) Heatmap for normalized enrichment scores (NESs) for comparing the response to lifespan-extending interventions in mice,[55] and the *APRT*$^{\Delta 8/+}$ old fish. The full pathway list is reported in Table S2.

(B) Experimental design for characterizing the livers of male and female fish using RNA-sequencing under basal metabolic conditions (i.e., fasting).

(C) Functional enrichments (GO) using GSEA for differential gene expression between old and young fish. GO enrichments using GSEA were called at FDR < 5%.

(D) Relative expression of driver genes from the pathways in (C). For each condition, the expression level is normalized to young WT. Significance was calculated using two-way ANOVA and Tukey post hoc.

**A** Liver metabolomic and lipidomic profiling during fasting in male fish

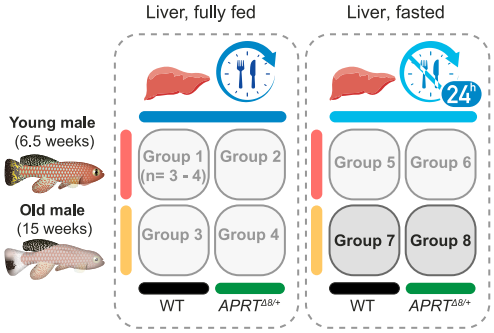


**B** An altered fasting response in old heterozygous male fish

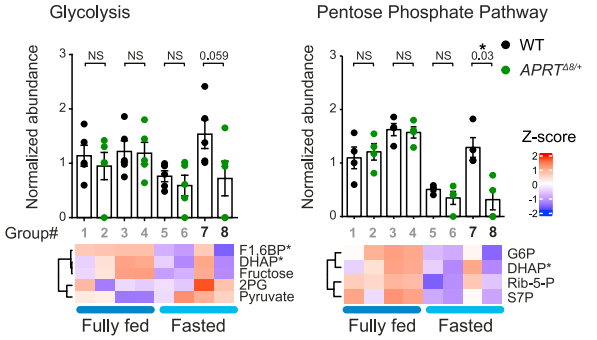


**C** Altered purine biosynthesis in old heterozygous male fish

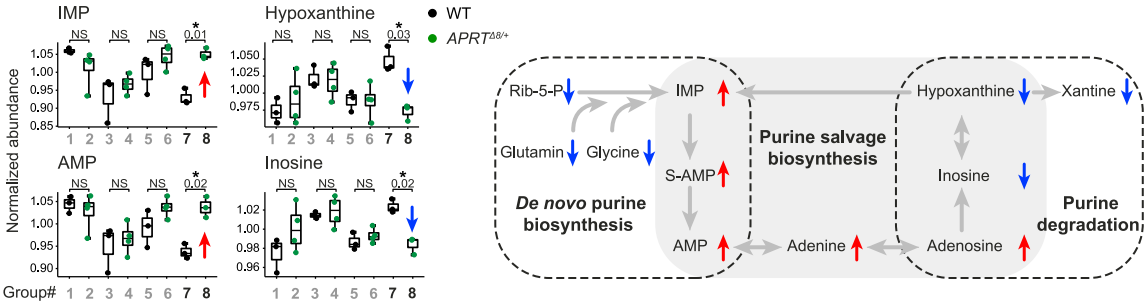


**D** Altered lipid metabolism during fasting in old heterozygous male fish

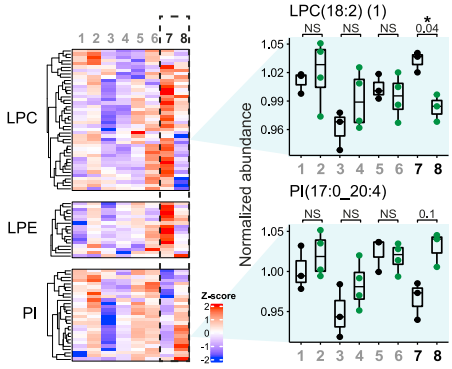


**E** Altered triacylglycerol biosynthesis (TG) in old heterozygous male fish

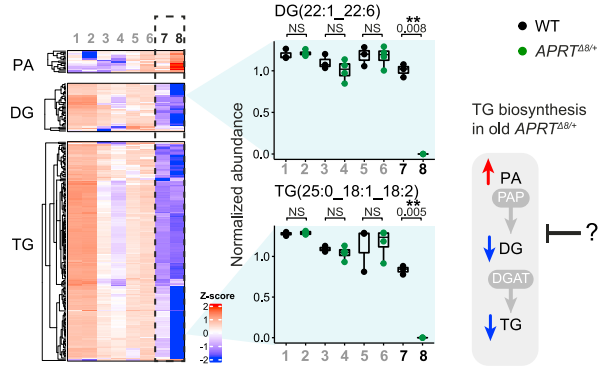


**F** Resistance to short-term high-fat diet in old heterozygous male fish

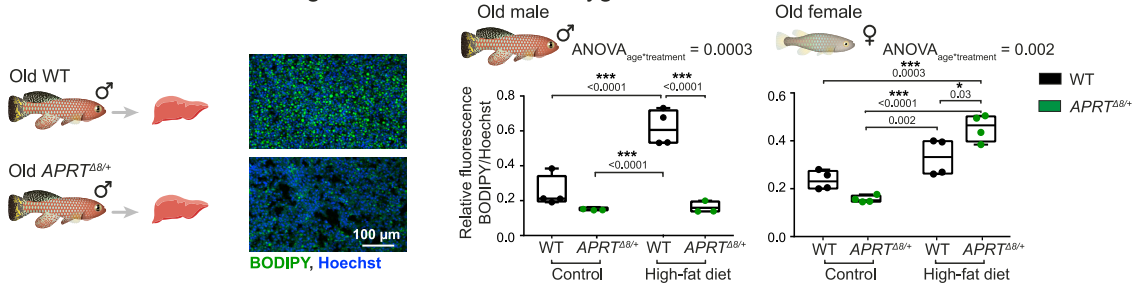


*(legend on next page)*

during fasting in old WT males (group #7), suggesting deregulated nutrient sensing. In contrast, this trend was not observed in old heterozygous fish (group #8), when compared with the corresponding old WT males (group #7, Figure 3B, top). Significant metabolites between groups #7 and #8 are highlighted with an Asterix (p value < 0.05, Figure 3B, bottom; see STAR Methods for statistical analysis). Similar trends were observed in members of primary energy and biosynthetic pathways, including the pentose phosphate pathway (PPP, Figure 3B, right), whereas other pathways, such as amino acid metabolism, displayed a modest trend (Figure S3B). The PPP is an integral part of the mammalian fasting response,[63–66] and inhibition of the PPP was recently shown to promote longevity in *C. elegans* by mimicking dietary restriction.[67]

How does APRT mutation affect nucleotide- and AMP-related metabolites? A global overview of nucleotide metabolism suggested that APRT haploinsufficiency broadly alters related metabolites (Figure S3C). However, an in-depth analysis highlighted a clear trend for purine metabolism, which includes AMP biosynthesis. Specifically, when compared with WT fish, old heterozygous fish upregulated purine salvage metabolites (including adenine and AMP). This upregulation comes at the expense of *de novo* purine biosynthesis or degradation (Figure 3C; adapted from Yin et al.[68]). Interestingly, similar trends were previously suggested as compensatory mechanisms during fasting.[69] Taken together, our metabolomic data suggest that with age, the *APRT*$^{\Delta 8/+}$ mutation affects nucleotide metabolism (e.g., by upregulating hepatic AMP salvage). Furthermore, WT males display reduced metabolic plasticity, which is partially restored in heterozygous fish.

## *APRT*$^{\Delta 8/+}$ male fish undergo a fasting-like inhibition of hepatic lipid accumulation

Our transcriptomic data also predict the involvement of lipid metabolism (Figure 1F). Therefore, we performed lipidomic profiling, using the same experimental design described above (Figure 3A). PCA demonstrated some age- and genotype-related segregation (i.e., PC1, Figure S3D). When comparing lipid profiles of old WT and *APRT*$^{\Delta 8/+}$ fish during fasting (groups #7 and #8, respectively), hierarchical clustering highlighted several lipid species (Figure S3E). For example, although PI (phosphatidylinositol) levels are downregulated in response to fasting in old WT fish (group #7), these trends are largely missing in old heterozygous fish (group #8) (Figure 3D). An opposite trend was also seen in lysophosphatidylcholine (LPC).

In contrast, many lipid species seem to specifically accumulate in heterozygous old fish, such as phosphatidic acids (PAs), whereas others were significantly depleted, such as TGs and DGs (triglycerols and diglycerols, respectively). PA, DG, and TG are part of triacylglycerol synthesis by the Kennedy pathway.[70] Our data suggest that triacylglycerol synthesis or accumulation might be inhibited (Figure 3E). To test if lipid droplet abundance is indeed altered *in-vivo*, we developed a short-term high-fat diet regimen, using hepatic lipid accumulation as a readout (Figure S3F). Applying this protocol to both sexes revealed that old *APRT*$^{\Delta 8/+}$ males are resistant to high-fat diets and maintained comparable hepatic lipid droplets with those of control fish (Figures 3F and S1F). These findings were also supported by the detailed histological characterization using H&E (Figure S1F; Table S1). Together, our multi-omic characterization, combined with either a short-term fasting or high-fat diet regimen, suggests that *APRT*$^{\Delta 8/+}$ male fish experience a fasting-like metabolic switch. However, the question of how other predicted cellular functions are affected, including mitochondrial dynamics (Figures 2A and 2C), remains.

## Inhibited mitochondrial functions in *APRT*$^{\Delta 8/+}$-derived cells can be rescued by adenine

Fasting promotes functional changes in the mitochondria, including reduced mitochondrial respiration in the liver[71] and increased biogenesis.[72] Therefore, to first explore mitochondrial respiration on a cellular level, we developed primary fibroblast cultures from WT and *APRT*$^{\Delta 8/+}$ males (Figure 4A). Optimizing previously published protocols[73] allowed us to produce robust early-passage cultures and use individual fish as biological replicates. *APRT*$^{\Delta 8/+}$-derived cells display reduced proliferation compared with WT cells, and as expected, they are partially resistant to 8-azaadenine treatment (Figure S4A). This resistance

**Figure 3. Heterozygous *APRT*$^{\Delta 8/+}$ mutation induces a metabolic switch**

(A) Experimental design for characterizing the livers of male fish using metabolomics and lipidomics.

(B) Bar plot (top) represents the normalized abundance of specific metabolites (BioCyc). Glycolysis includes primary glycolytic metabolites. Each dot represents averaged biological replicates (3–4 fish per experimental group). Bars represent mean ± SEM. Significance was called by unpaired two-sided t test between the WT and *APRT*$^{\Delta 8/+}$ in each experimental condition (age and feeding) with FDR correction. Heatmap (bottom) of the top significant metabolites between groups #7 and #8 as described above. Values are represented as *Z* score. F1,6BP, beta-D-Fructose 1,6-bisphosphate; DHAP, dihydroxyacetone phosphate; 2PG, 2-phospho-D-glycerate; G6P, glucose 6-phosphate; Rib-5-P, ribose-5-phosphate; S7P, sedoheptulose 7-phosphate; and G1P, glucose 1-phosphate.

(C) Left: boxplot showing key metabolites from the nucleoside and nucleotide metabolism pathways (BioCyc). All metabolites are presented in Figure S3C. Whiskers represent minimum and maximum. Significance was called by unpaired two-sided t test and FDR correction between the WT and *APRT*$^{\Delta 8/+}$ in each experimental condition. Right: a diagram of purine metabolism. The red and blue arrows correspond to the changes between groups #7 and #8.

(D) Heatmap (left) showing lipid species that display an altered age-related fasting response (i.e., LPC, LPE, and PI). Each square represents normalized relative abundance (by color), from an average of 3–4 fish. Boxplot (right) for significantly altered lipid species. Significance was called by unpaired two-sided t test between the WT and *APRT*$^{\Delta 8/+}$ in each experimental condition (age and feeding) with FDR correction. LPC, lysophosphatidylcholine; LPE, lysophosphatidylethanolamine; PI, phosphatidylinositol.

(E) Heatmap (left) showing lipid species that are a part of TG biosynthesis. Heatmap and boxplot (center) are calculated as described in (D). A diagram for TG biosynthesis via the Kennedy pathway (right), depicting key enzymes and primary lipid species. PA, phosphatidic acid; DG, diacylglycerol; TG, triacylglycerol; PAP, phosphatidate phosphatase; DGAT, diacylglycerol acyltransferase.

(F) Hepatic lipid accumulation in response to high-fat diets. Left: BODIPY staining (green) and nuclei (blue) in liver sections. Scale bar represents 100 μm. Right: boxplot for the quantification of the relative fluorescence intensity of BODIPY/Hoechst at the indicated experimental groups. n ≥ 3 biological replicates of each group. Significance was calculated using two-way ANOVA and Tukey post hoc. Exact p values are indicated.

Unless stated otherwise, each symbol represents an individual fish, and Whisker plot represents minimum and maximum.

**A** Generation of fibroblast primary cell culture

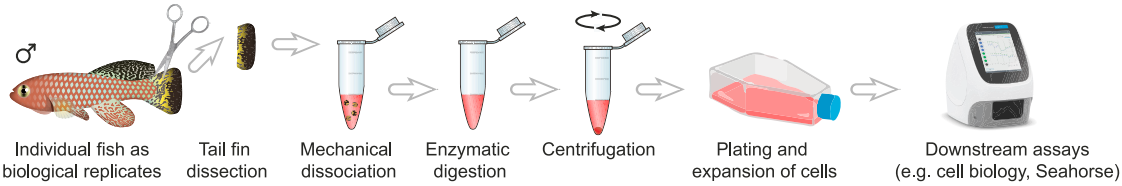


**B** Reduced mitochondrial respiration in *APRT*$^{\Delta 8/+}$-derived cells

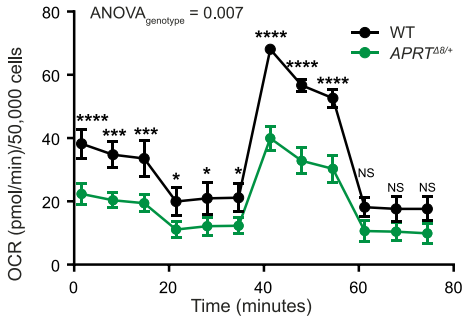


**C** Mitochondrial functions in primary cells

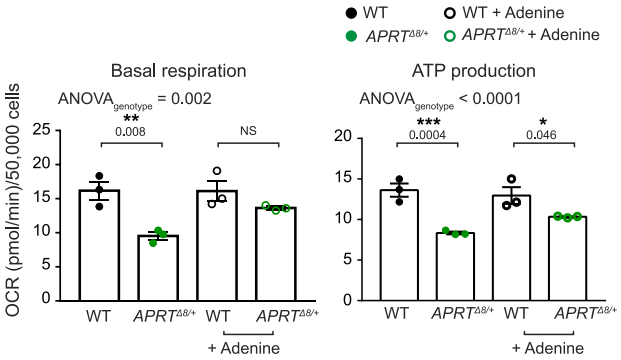


**D** AMPK pathway activation in WT and *APRT*$^{\Delta 8/+}$-derived cells

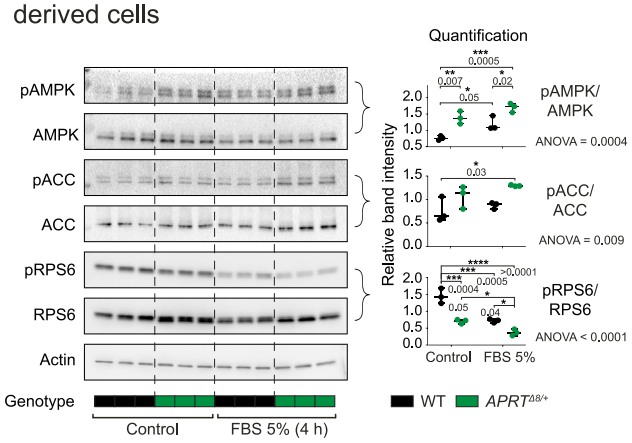


**E** Altered nucleotide pool in *APRT*$^{\Delta 8/+}$-derived cells

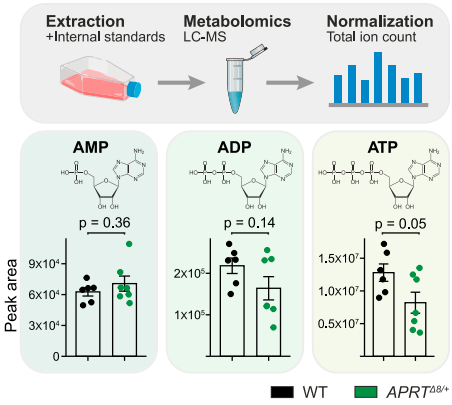


**F** Lifespan of WT and *APRT*$^{\Delta 8/+}$ fish under intermittent fasting

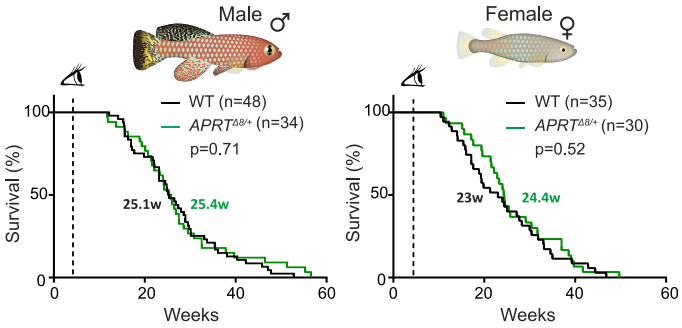


**G** Model

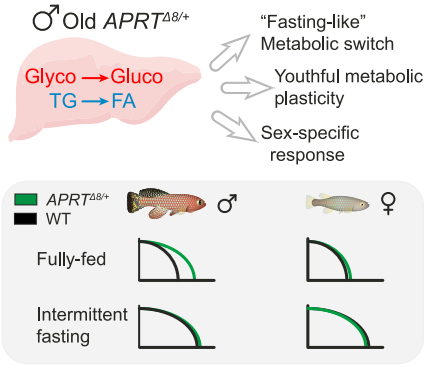


*(legend on next page)*

is a consequence of the reduced ability to metabolize adenine and therefore to produce the toxic intermediate generated by metabolizing 8-azaadenine.[74,75]

We then used the seahorse platform to characterize mitochondrial functions ("Mito Stress" assay, Figures 4B, 4C, and S4B). Our results indicated that mitochondrial respiration (including ATP production) and glycolytic functions were significantly reduced in *APRT*$^{\Delta 8/+}$-derived cells (Figures 4B, 4C, S4C, and S4D). We hypothesized that the observed phenotypes could be rescued by exogenously manipulating the nucleotide pools. APRT catalyzes the formation of AMP by using adenine as a precursor. Accordingly, supplementing adenine can restore mitochondrial functions in heterozygous cells by rescuing respiration (Figure 4C). Characterization of mitochondrial morphology revealed that although mitochondrial branch length is slightly increased in heterozygous cells, mitochondrial footprint was overall unaffected (Figure S4E). Together, our findings suggest that the *APRT*$^{\Delta 8/+}$ mutation is associated with reduced mitochondrial functions. These phenotypes are a conserved fasting response[71] and are tightly linked to longevity mechanisms.[76–78]

## Increased mitochondrial copy numbers in *APRT*$^{\Delta 8/+}$ male fish

To explore whether the fasting-like response also affects mitochondrial biogenesis, we investigated mitochondrial copy numbers. *PGC-1*$\alpha$, also known as *PPARGC1A* (peroxisome proliferator-activated receptor gamma coactivator 1-$\alpha$), is a master regulator of mitochondrial biogenesis and an AMPK target.[18] Accordingly, *PGC-1*$\alpha$ transcripts were upregulated in heterozygous males (Figure 1F), and an increase in mitochondrial DNA (mtDNA) copy number was detected in both livers and tails of old male *APRT*$^{\Delta 8/+}$ fish (Figure S4F, left and center).

The higher mitochondrial numbers observed in heterozygous old males were similar to the already high numbers in females (Figure S4F). These data raise the possibility that as previously suggested for other sex-biased liver functions,[79,80] circulating factors (e.g., sex hormones) could be involved. In support of these findings is the proposed feminizing effect in *APRT*$^{\Delta 8/+}$ fish (Figure 2A), and the fact that in primary cultured fibroblasts (male or females), this phenotype was lost (Figure S4F, right). To functionally explore this link, we performed a short-term exposure to estradiol (E2) in fish, which significantly increased mitochondrial copy numbers in the liver, specifically in males (Figure S4G). Thus, our findings suggest that some fasting-like phenotypes, such as an increase in male mitochondrial copy numbers, might depend on a physiological context (e.g., sex-dimorphic energy partitioning or circulating factors; Figures 2C, 2D, and S2F–S2H). Next, we wished to directly explore the activation state of the AMPK pathway.

## Altered cellular nucleotide ratios correlate with an increased AMPK activity in *APRT*$^{\Delta 8/+}$-derived cells

To investigate our findings on the protein level, we first validated a panel of specific antibodies directed against key members of the vertebrate fasting response and classical AMPK targets (Figures S5A and S5B; see STAR Methods). Our results indicate that under control conditions, *APRT*$^{\Delta 8/+}$-derived cells display a significant activation of the AMPK pathway, which resembles the activation observed in WT cells under serum starvation (Figure 4D). In heterozygous cells, this increase is further heightened under serum starvation, suggesting that the *APRT*$^{\Delta 8/+}$ mutation can sensitize cells to nutrient levels and induce a fasting-like state. In livers, a genotype-dependent response to fasting was also observed at the protein level, which was evaluated by phosphorylation levels of ribosomal protein S6 (pRPS6, Figure S5C). These findings are in agreement with a signature of mTOR inhibition, which was observed in the liver of old heterozygous male fish (i.e., rapamycin, Figure 2A).[81]

To directly quantify the relative abundance of AMP, ADP, and ATP, we analyzed primary cultures by liquid chromatography mass spectrometry (LC-MS). The results revealed that ATP levels are significantly decreased in *APRT*$^{\Delta 8/+}$-derived cells ($p = 0.05$, t test), although there was a trending decrease in ADP ($p = 0.14$, t test) and no change in AMP levels (Figure 4E). It is known that assessing the levels of individual nucleotides could be misleading, as they exist in a steady state with other biosynthetic pathways. Therefore, we compared the nucleotide ratio of AMP:ATP between WT and *APRT*$^{\Delta 8/+}$ as follows:

**Figure 4. Intermittent fasting abolishes the male-specific longevity benefits of the *APRT*$^{\Delta 8/+}$ mutation**

(A) Schematic illustration depicting the isolation procedure of primary fibroblasts from the tail-fin of individual male fish (n = 3 for each genotype).

(B) Measuring mitochondrial respiration in WT- and *APRT*$^{\Delta 8/+}$-derived primary cells according to Figure S4B. Experiments were performed in control conditions. Each symbol represents an average of three independent measurements using cells derived from three individual fish. Error bars represent mean ± SEM, and significance was measured by two-way repeated measures ANOVA and Sidak correction.

(C) Basal respiration and ATP production were compared between WT- and *APRT*$^{\Delta 8/+}$-derived primary cells following adenine supplementation. Error bars represent mean ± SEM, and significance was measured by two-way ANOVA and Tukey post hoc.

(D) Western blot (left) for members of the AMPK signaling pathway, in WT- and *APRT*$^{\Delta 8/+}$-derived primary cells (n = 3). Quantification (Fiji/ImageJ, right) represents the ratio between the phosphorylated and non-phosphorylated forms. Dot plot represents the quantification of the western blot (WB). Significance was calculated using two-way ANOVA and Tukey post hoc, and the interaction value between the genotype and the experimental treatment are presented. Exact p values are indicated. AMPK, AMPK$\alpha$; pAMPK, phospho-AMPK$\alpha$ (Thr172); ACC, acetyl-CoA carboxylase; pACC, phospho-acetyl-CoA carboxylase (Ser79); RPS6, S6 ribosomal protein; pRPS6, phospho-S6 ribosomal protein (Ser235/236).

(E) Direct measurement of the nucleotide pool using LC-MS, for relative concentration of AMP, ADP, and ATP in WT- and *APRT*$^{\Delta 8/+}$-derived primary cells. Data were obtained from 6 to 7 biological replicates for each experimental condition, and normalized by total ion count (TIC). Bar plot representing mean ± SEM, unpaired two-sided t test and exact p values are indicated.

(F) Lifespan of WT (black) and *APRT*$^{\Delta 8/+}$ (green) fish performed separately for males (left) and females (right) under lifelong intermittent fasting conditions. Lifespan records were initiated at 4 weeks (eye symbol). p values for differential survival in log rank tests, median survival, and cohort size are indicated.

(G) Top: a schematic model proposing that APRT, a member of the AMP biosynthesis pathway, can function as a regulator for vertebrate longevity. Gly, glycolysis; Glu, gluconeogenesis; TG, triglyceride. Bottom: male-specific longevity benefits are abolished by lifelong intermittent fasting.

For cell culture experiments, data were obtained from 3 independent primary cultures per genotype.

$\frac{AMP^{Het}}{ATP^{Het}}/\frac{AMP^{WT}}{ATP^{WT}}$ = 1.8. This ratio indicated an energy starvation state in mutant cells, which was abrogated following adenine supplementation (nucleotide ratio = 1.07, Table S4). Similarly, adenine supplementation also increased ATP levels via APRT in a mammalian wound healing model[82] and abrogated the longevity effects of an *ADSS* mutant (adenylosuccinate synthetase) in *Drosophila*.[26]

Overall, these data imply that on the cellular level, *APRT*$^{\Delta 8/+}$-derived cells exist at a low energy state associated with an activated AMPK pathway. We were next curious to test whether the genetically induced fasting-like state in *APRT*$^{\Delta 8/+}$ heterozygous males could be linked to longevity phenotypes.

### Intermittent fasting abolishes the longevity benefits mediated by *APRT*

Our findings so far have led us to hypothesize that the longevity benefits in *APRT*$^{\Delta 8/+}$ males could be negated by fasting, which is predicted to induce an equivalent fasting response in WT fish. Excitingly, although the lifespan of both male and female fish was significantly extended following lifelong intermittent fasting (~70% increase in median lifespan, Figure S5D), we could not detect any further extension in *APRT*$^{\Delta 8/+}$ male fish (log rank test, p = 0.71, Figure 4F).

Together, our findings demonstrate that mutating *APRT*, a member of the AMP salvage pathway, produced a pro-longevity effect in males. This effect could be abrogated by intermittent fasting. Furthermore, the observed longevity benefits are accompanied by several physiological and cellular phenotypes, including restoration of metabolic plasticity, a fasting-like state, and activation of AMPK downstream targets. In conclusion, our data suggest that genetic perturbation of the AMP salvage pathway can regulate metabolic health and longevity in killifish, a vertebrate model for aging (Figure 4G).

## DISCUSSION

Here, to explore the involvement of the AMP/AMPK axis in vertebrate longevity, we use the emerging turquoise killifish model. By mutating APRT, a key enzyme in AMP biosynthesis, we demonstrate that heterozygous males are long-lived. To better understand the molecular mechanism behind the observed longevity effect, which are possibly sex-dimorphic, we use an integrated omics approach in primary metabolic organs, characterize related cellular phenotypes, develop dietary and pharmacological interventions, investigate the AMP biosynthesis pathway in killifish and humans, and compare the APRT mutation with a comprehensive panel of longevity interventions in mice.

Specifically, we demonstrate that age-related loss of metabolic homeostasis is restored in male mutants. These phenotypes are accompanied by a fasting-like metabolic switch and modified mitochondrial dynamics. On the cellular level, this genetically induced starvation state was associated with reduced ATP levels and activated the AMPK pathway. Finally, lifelong intermittent fasting abolished the longevity benefits. These observations suggest that genetic perturbation of APRT might alter the nucleotide pool of the AMP/AMPK axis, which in turn, can affect lifespan and metabolism. Furthermore, we provide intriguing insights into the mechanisms behind sex differences in longevity. It is worth mentioning that although our transcriptomic analysis highlighted sex-dimorphic patterns in heterozygous mutants, these changes may be correlative, and additional epistasis experiments will be required in the future.

Our findings highlight an age/genotype-dependent fasting-like switch that separates male and female physiology. Sexual dimorphism in metabolic pathways, which has been primarily studied in young animals, is evolutionarily linked to the distinct energy requirements during reproductive life.[10,80,83–86] With age, these characteristics might also contribute to the sex biases in genetic longevity mechanisms[5,87–91] and to the differential predisposition to various age-related diseases (e.g., type 2 diabetes).[15,16] Accordingly, pharmacological longevity interventions, such as metformin,[92] can produce sex-biased effects (https://phenome.jax.org/projects/ITP1), and the benefits of dietary restriction are thought to be mediated by sex-specific responses.[93] Therefore, focusing on sexually dimorphic mechanisms is important for developing personalized perturbations (e.g., in human trials).[94,95]

The longevity effects of intermittent fasting were dominant over the effect mediated by the APRT mutation. Furthermore, this must be reconciled with the observation that intermittent fasting equally affects the lifespan of both sexes, whereas APRT has an impact primarily on male fish. A possible explanation for the observed sexual dimorphism could be the sex differences in purine metabolism (e.g., NT5C2 in Figure S2H and Table S2), data in humans,[62] and the increased susceptibility of male mice to a complete APRT deficiency.[96]

Another possibility could be that the beneficial effects of dietary restriction are mediated by systemic sex-specific mechanisms.[5,93] Some of these mechanisms, such as sex hormones[80] (Figures 2A and S4G), were previously shown to interact with AMPK.[97] Furthermore, supporting this hypothesis is the naturally higher activity of AMPK observed in female rat livers[98] and invertebrate models.[99] Thus, females might not be able to further enhance metabolic functions via AMPK, whereas males have a better dynamic range.

AMP salvage is predicted to be the primary source (~90%) of daily purine nucleotide biosynthesis across different organs.[82,100–102] Our findings propose the APRT enzyme as a promising pharmacological target for replicating the benefits of fasting and promoting vertebrate longevity. However, although significant efforts have been invested in *Leishmania* research,[103] a selective APRT inhibitor is still missing. Along these same lines, *APRT* heterozygous fish display distinct compositional changes in the subunits of the AMPK complex (Figure S1J). Previous observations suggest that distinct subunit compositions can allow the AMPK complexes to produce a tailored response.[20,104] Thus, our findings provide the basis for future direct interventions in AMPK subunits.

Intriguingly, APRT heterozygosity is predicted to actually reduce AMP levels and therefore decrease AMP:ATP ratios. Thus, the observed AMPK activation state could seem counterintuitive under stable conditions.[26,105] However, our data in cells confirm that the AMP:ATP ratio indeed increases, mostly due to the reduction in ATP (Figure 4E). *In-vivo*, our metabolomics findings suggest that the AMP salvage pathway is upregulated, specifically in old fish, as a possible compensatory mechanism (Figure 3C).[69] Furthermore, predicting the precise effect on AMP levels is

non-intuitive, as it is in a steady state with other nucleotides, as was previously demonstrated in an *APRT* mutation in *Drosophila*.[26]

Thus, we speculate that under low AMP production rates, the cell and the organism are more sensitive to spikes in energy consumption. Specifically, such spikes can include cell division (which can give rise to slower proliferation; Figure S4A), rapid organismal growth (e.g., leading to a smaller size; Figure S1E), and naturally occurring variations in fasting and refeeding cycles (Figure 4D). Together, our findings provide a global understanding of how nucleotide biosynthesis can affect the AMP/AMPK axis and regulate metabolism and longevity in a vertebrate model.

### Limitations of the study

It is worth mentioning that during intermittent fasting, fish were restricted to one meal a day, in which they could feed *ad libitum*. Thus, we cannot exclude the possibility that they were also under dietary/CR. Furthermore, although heterozygous male fish are smaller than wild types, our current experimental design did not allow us to investigate how the size differences themselves impact metabolic or gene expression changes.

## STAR★METHODS

Detailed methods are provided in the online version of this paper and include the following:

- KEY RESOURCES TABLE
- RESOURCE AVAILABILITY
  - Lead contact
  - Materials availability
  - Data and code availability
- EXPERIMENTAL MODEL AND SUBJECT DETAILS
  - African turquoise killifish strain, husbandry, and maintenance
  - CRISPR/Cas9 target prediction and gRNA synthesis
  - Production of Cas9 mRNA
  - Microinjection of turquoise killifish embryos and generation of mutant fish using CRISPR/Cas9
  - Generation of primary fibroblast cultures from killifish tail fins
- METHOD DETAILS
  - Organ isolation
  - Lipid and polar metabolic profiling
  - RNA sequencing
  - Survival, maturity, and growth assays
  - Fertility analysis
  - Histology
  - Dietary manipulations
  - Seahorse metabolic extracellular flux profiling
  - Pharmacological manipulation of cultured cells
  - Mitochondrial morphology
  - LC-MS for direct quantification of AMP, ADP, and ATP
  - Protein gel electrophoresis and immunoblotting
  - DNA isolation and measurement of mitochondrial DNA content using quantitative PCR
  - A-to-I RNA editing
- QUANTIFICATION AND STATISTICAL ANALYSIS
  - Statistics tests

## SUPPLEMENTAL INFORMATION

Supplemental information can be found online at https://doi.org/10.1016/j.devcel.2023.05.015.

## ACKNOWLEDGMENTS

We thank the Harel lab, Sagiv Shifman, Tamar Avin-Wittenberg, Eran Meshorer, Anne Brunet, and Berenice Benayoun for stimulating discussion and feedback on the manuscript. We thank Ella Yanay and Ashayma Abutair for help with killifish maintenance, Yaakov Nahmias and Konstantinos Ioannidis for help with the Seahorse assay, Naomi Melamed-Book and Rachel Rosen from the core facilities (HUJI), Ifat Abramovich, Bella Agranovich, Eyal Gottlieb, Sergey Malitsky, and Maxim Itkin for help with mass spectrometry, and Param Priya Singh and Anne Brunet for advice with the GSEA code. Supported by the Zuckerman Program (I.H.), Abisch-Frenkel Foundation 19/HU04 (I.H.), Switzerland, ISF 2178/19 (I.H.), Israel Ministry of Science 3-17631 (I.H.), 3-16872 (I.H.), the Moore Foundation GBMF9341 (I.H.), United States, BSF-NSF 2020611 (I.H.), the Israel Ministry of Agriculture 12-16-0010 (I.H), ERC StG #101078188 (I.H), and the Lady Davis Postdoctoral Fellowship (G.A.).

## AUTHOR CONTRIBUTIONS

Conceptualization, G.A., T.A., and I.H.; methodology, G.A., T.A., and A.V.; software, T.A. and K.S.; validation, G.A., T.A., and I.H.; formal analysis, T.A., G.A., J.D., K.S., E.Y.L., and I.H.; investigation, G.A., U.G., A.O.-G., T.A., T.L., and M.S.; resources, data curation, writing—original draft, G.A., T.A., and I.H.; writing—review and editing, T.A. and I.H.; visualization, T.A. and G.A.; supervision, I.H. and E.Y.L.; project administration, G.A. and T.A.; funding acquisition, I.H.

## DECLARATION OF INTERESTS

The authors declare no competing interests.

## INCLUSION AND DIVERSITY

We support inclusive, diverse, and equitable conduct of research.

Received: September 27, 2022
Revised: March 9, 2023
Accepted: May 23, 2023
Published: June 14, 2023

## REFERENCES

1. Finkel, T. (2015). The metabolic regulation of aging. Nat. Med. *21*, 1416–1423.
2. Niccoli, T., and Partridge, L. (2012). Ageing as a risk factor for disease. Curr. Biol. *22*, R741–R752. https://doi.org/10.1016/j.cub.2012.07.024.
3. Amorim, J.A., Coppotelli, G., Rolo, A.P., Palmeira, C.M., Ross, J.M., and Sinclair, D.A. (2022). Mitochondrial and metabolic dysfunction in ageing and age-related diseases. Nat. Rev. Endocrinol. *18*, 243–258.
4. Lopez-Otin, C., Blasco, M.A., Partridge, L., Serrano, M., Kroemer, G., López-Otín, C., Blasco, M.A., Partridge, L., Serrano, M., and Kroemer, G. (2013). The hallmarks of aging. Cell *153*, 1194–1217. https://doi.org/10.1016/j.cell.2013.05.039.
5. Green, C.L., Lamming, D.W., and Fontana, L. (2022). Molecular mechanisms of dietary restriction promoting health and longevity. Nat. Rev. Mol. Cell Biol. *23*, 56–73.
6. Smith, H.J., Sharma, A., and Mair, W.B. (2020). Metabolic communication and healthy aging: where should we focus our energy? Dev. Cell *54*, 196–211.
7. de Cabo, R., Carmona-Gutierrez, D., Bernier, M., Hall, M.N., and Madeo, F. (2014). The search for antiaging interventions: from elixirs to fasting regimens. Cell *157*, 1515–1526.

8. Soeters, M.R., Sauerwein, H.P., Groener, J.E., Aerts, J.M., Ackermans, M.T., Glatz, J.F.C., Fliers, E., and Serlie, M.J. (2007). Gender-related differences in the metabolic response to fasting. J. Clin. Endocrinol. Metab. *92*, 3646–3652.
9. Morris, A. (2021). Sex differences for fasting levels of glucose and insulin: expanding our understanding. Nat. Rev. Endocrinol. *17*, 131.
10. Bazhan, N., Jakovleva, T., Feofanova, N., Denisova, E., Dubinina, A., Sitnikova, N., and Makarova, E. (2019). Sex differences in liver, adipose tissue, and muscle transcriptional response to fasting and refeeding in mice. Cells *8*, 1529.
11. De Cabo, R., and Mattson, M.P. (2019). Effects of intermittent fasting on health, aging, and disease. N. Engl. J. Med. *381*, 2541–2551.
12. Wu, B.N., and O'Sullivan, A.J. (2011). Sex differences in energy metabolism need to be considered with lifestyle modifications in humans. J. Nutr. Metab. *2011*, 391809.
13. Link, J.C., and Reue, K. (2017). Genetic basis for sex differences in obesity and lipid metabolism. Annu. Rev. Nutr. *37*, 225–245.
14. Mauvais-Jarvis, F., Arnold, A.P., and Reue, K. (2017). A guide for the design of pre-clinical studies on sex differences in metabolism. Cell Metab. *25*, 1216–1230.
15. Tramunt, B., Smati, S., Grandgeorge, N., Lenfant, F., Arnal, J.-F., Montagner, A., and Gourdy, P. (2020). Sex differences in metabolic regulation and diabetes susceptibility. Diabetologia *63*, 453–461.
16. Hägg, S., and Jylhävä, J. (2021). Sex differences in biological aging with a focus on human studies. eLife *10*, e63425.
17. Austad, S.N., and Fischer, K.E. (2016). Sex differences in lifespan. Cell Metab. *23*, 1022–1033.
18. Garcia, D., and Shaw, R.J. (2017). AMPK: mechanisms of cellular energy sensing and restoration of metabolic balance. Mol. Cell *66*, 789–800.
19. Hardie, D.G., Ross, F.A., and Hawley, S.A. (2012). AMPK: a nutrient and energy sensor that maintains energy homeostasis. Nat. Rev. Mol. Cell Biol. *13*, 251–262.
20. Herzig, S., and Shaw, R.J. (2018). AMPK: guardian of metabolism and mitochondrial homeostasis. Nat. Rev. Mol. Cell Biol. *19*, 121–135.
21. Bideyan, L., Nagari, R., and Tontonoz, P. (2021). Hepatic transcriptional responses to fasting and feeding. Genes Dev. *35*, 635–657.
22. Trefts, E., Gannon, M., and Wasserman, D.H. (2017). The liver. Curr. Biol. *27*, R1147–R1151. https://doi.org/10.1016/j.cub.2017.09.019.
23. Berg, J.M., Tymoczko, J.L., and Stryer, L. (2002). Biochemistry (W. H. Freeman Publishing).
24. Burkewitz, K., Zhang, Y., and Mair, W.B. (2014). AMPK at the nexus of energetics and aging. Cell Metab. *20*, 10–25.
25. Ulgherait, M., Rana, A., Rera, M., Graniel, J., and Walker, D.W. (2014). AMPK modulates tissue and organismal aging in a non-cell-autonomous manner. Cell Rep. *8*, 1767–1780.
26. Stenesen, D., Suh, J.M., Seo, J., Yu, K., Lee, K.-S., Kim, J.-S., Min, K.-J., and Graff, J.M. (2013). Adenosine nucleotide biosynthesis and AMPK regulate adult life span and mediate the longevity benefit of caloric restriction in flies. Cell Metab. *17*, 101–112.
27. Apfeld, J., O'Connor, G., McDonagh, T., DiStefano, P.S., and Curtis, R. (2004). The AMP-activated protein kinase AAK-2 links energy levels and insulin-like signals to lifespan in C. elegans. Genes Dev. *18*, 3004–3009.
28. Curtis, R., O'Connor, G., and DiStefano, P.S. (2006). Aging networks in Caenorhabditis elegans: AMP-activated protein kinase (aak-2) links multiple aging and metabolism pathways. Aging Cell *5*, 119–126.
29. Greer, E.L., Dowlatshahi, D., Banko, M.R., Villen, J., Hoang, K., Blanchard, D., Gygi, S.P., and Brunet, A. (2007). An AMPK-FOXO pathway mediates longevity induced by a novel method of dietary restriction in C. elegans. Curr. Biol. *17*, 1646–1656.
30. Mair, W., Morantte, I., Rodrigues, A.P.C., Manning, G., Montminy, M., Shaw, R.J., and Dillin, A. (2011). Lifespan extension induced by AMPK and calcineurin is mediated by CRTC-1 and CREB. Nature *470*, 404–408.
31. Matecic, M., Smith, D.L., Jr., Pan, X., Maqani, N., Bekiranov, S., Boeke, J.D., and Smith, J.S. (2010). A microarray-based genetic screen for yeast chronological aging factors. PLOS Genet. *6*, e1000921.
32. Lin, J.-R., Sin-Chan, P., Napolioni, V., Torres, G.G., Mitra, J., Zhang, Q., Jabalameli, M.R., Wang, Z., Nguyen, N., and Gao, T. (2021). Rare genetic coding variants associated with human longevity and protection against age-related diseases. Nat. Aging *1*, 783–794.
33. Carling, D. (2017). AMPK signalling in health and disease. Curr. Opin. Cell Biol. *45*, 31–37.
34. Yang, X., Mudgett, J., Bou-About, G., Champy, M.-F., Jacobs, H., Monassier, L., Pavlovic, G., Sorg, T., Herault, Y., and Petit-Demoulière, B. (2016). Physiological expression of AMPK$\gamma$2RG mutation causes Wolff-Parkinson-White syndrome and induces kidney injury in mice. J. Biol. Chem. *291*, 23428–23439.
35. Yavari, A., Stocker, C.J., Ghaffari, S., Wargent, E.T., Steeples, V., Czibik, G., Pinter, K., Bellahcene, M., Woods, A., and De Morentin, P.B.M. (2016). Chronic activation of $\gamma$2 AMPK induces obesity and reduces $\beta$ cell function. Cell Metab. *23*, 821–836.
36. Woods, A., Williams, J.R., Muckett, P.J., Mayer, F.V., Liljevald, M., Bohlooly-Y, M., and Carling, D. (2017). Liver-specific activation of AMPK prevents steatosis on a high-fructose diet. Cell Rep. *18*, 3043–3051.
37. Harel, I. (2022). The turquoise killifish. Nat. Methods *19*, 1150–1151. https://doi.org/10.1038/s41592-022-01631-y.
38. Harel, I., and Brunet, A. (2015). The African turquoise killifish: A model for exploring vertebrate aging and diseases in the fast Lane. Cold Spring Harb. Symp. Quant. Biol. *80*, 275–279. https://doi.org/10.1101/sqb.2015.80.027524.
39. Kim, Y., Nam, H.G., and Valenzano, D.R. (2016). The short-lived African turquoise killifish: an emerging experimental model for ageing. Dis. Model. Mech. *9*, 115–129. https://doi.org/10.1242/dmm.023226.
40. Cellerino, A., Valenzano, D.R., and Reichard, M. (2016). From the bush to the bench: the annual Nothobranchius fishes as a new model system in biology. Biol. Rev. Camb. Philos. Soc. *91*, 511–533. https://doi.org/10.1111/brv.12183.
41. Valenzano, D.R., Benayoun, B.A., Singh, P.P., Zhang, E., Etter, P.D., Hu, C.K., Clément-Ziza, M., Willemsen, D., Cui, R., Harel, I., et al. (2015). The African turquoise killifish genome provides insights into evolution and genetic architecture of lifespan. Cell *163*, 1539–1554. https://doi.org/10.1016/j.cell.2015.11.008.
42. Harel, I., Valenzano, D.R., and Brunet, A. (2016). Efficient genome engineering approaches for the short-lived African turquoise killifish. Nat. Protoc. *11*, 2010–2028. https://doi.org/10.1038/nprot.2016.103.
43. Harel, I., Benayoun, B.A., Machado, B., Singh, P.P., Hu, C.K., Pech, M.F., Valenzano, D.R., Zhang, E., Sharp, S.C., Artandi, S.E., et al. (2015). A platform for rapid exploration of aging and diseases in a naturally short-lived vertebrate. Cell *160*, 1013–1026. https://doi.org/10.1016/j.cell.2015.01.038.
44. Astre, G., Moses, E., and Harel, I. (2022). The African turquoise killifish (Nothobranchius furzeri): biology and research applications. In Laboratory Fish in Biomedical Research (Elsevier), pp. 245–287.
45. Rozenberg, I., Moses, E., and Harel, I. (2023). CRISPR–Cas9 Genome Editing in Nothobranchius furzeri for Gene Knockout and Knock-In. Cold Spring Harb. Protoc. *2023*, 90–99.
46. Moses, E., and Harel, I. (2023). A scalable platform for functional interrogation of peptide hormones in fish. https://doi.org/10.1101/2023.01.19.52467.
47. Rozenberg, I., Atlan, T., Franek, R., Moses, E., Oron-Gottesman, A., Chrzanowski, H., and Harel, I. (2023). Exploring life-long tissue homeostasis through lineage tracing and cell transplantation. https://doi.org/10.1101/2023.05.01.538839.
48. Wang, C., Li, Q., Redden, D.T., Weindruch, R., and Allison, D.B. (2004). Statistical methods for testing effects on "maximum lifespan.". Mech. Ageing Dev. *125*, 629–632.

49. Austad, S.N. (2006). Why women live longer than men: sex differences in longevity. Gend. Med. *3*, 79–92.
50. Horstman, A.M., Dillon, E.L., Urban, R.J., and Sheffield-Moore, M. (2012). The role of androgens and estrogens on healthy aging and longevity. J. Gerontol. Ser. A Biomed. Sci. Med. Sci. *67*, 1140–1152.
51. Hänzelmann, S., Castelo, R., and Guinney, J. (2013). GSVA: gene set variation analysis for microarray and RNA-seq data. BMC Bioinformatics *14*, 7.
52. Fabregat, A., Jupe, S., Matthews, L., Sidiropoulos, K., Gillespie, M., Garapati, P., Haw, R., Jassal, B., Korninger, F., and May, B. (2018). The reactome pathway KnowledgeBase. Nucleic Acids Res. *46*, D649–D655.
53. Anton, S.D., Moehl, K., Donahoo, W.T., Marosi, K., Lee, S.A., Mainous, A.G., III, Leeuwenburgh, C., and Mattson, M.P. (2018). Flipping the metabolic switch: understanding and applying the health benefits of fasting. Obesity (Silver Spring) *26*, 254–268.
54. Rui, L. (2014). Energy metabolism in the liver. Compr. Physiol. *4*, 177–197.
55. Tyshkovskiy, A., Bozaykut, P., Borodinova, A.A., Gerashchenko, M.V., Ables, G.P., Garratt, M., Khaitovich, P., Clish, C.B., Miller, R.A., and Gladyshev, V.N. (2019). Identification and application of gene expression signatures associated with lifespan extension. Cell Metab. *30*, 573–593.e8.
56. Benayoun, B.A., Pollina, E.A., Singh, P.P., Mahmoudi, S., Harel, I., Casey, K.M., Dulken, B.W., Kundaje, A., and Brunet, A. (2019). Remodeling of epigenome and transcriptome landscapes with aging in mice reveals widespread induction of inflammatory responses. Genome Res. *29*, 697–709. https://doi.org/10.1101/gr.240093.118.
57. Franceschi, C., Garagnani, P., Parini, P., Giuliani, C., and Santoro, A. (2018). Inflammaging: a new immune–metabolic viewpoint for age-related diseases. Nat. Rev. Endocrinol. *14*, 576–590.
58. Murphy, L.J. (2000). Overexpression of insulin-like growth factor binding protein-1 in transgenic mice. Pediatr. Nephrol. *14*, 567–571.
59. Schaum, N., Lehallier, B., Hahn, O., Pálovics, R., Hosseinzadeh, S., Lee, S.E., Sit, R., Lee, D.P., Losada, P.M., and Zardeneta, M.E. (2020). Ageing hallmarks exhibit organ-specific temporal signatures. Nature *583*, 596–602.
60. Kulkarni, S.S., Karlsson, H.K.R., Szekeres, F., Chibalin, A.V., Krook, A., and Zierath, J.R. (2011). Suppression of 5′-nucleotidase enzymes promotes AMP-activated protein kinase (AMPK) phosphorylation and metabolism in human and mouse skeletal muscle. J. Biol. Chem. *286*, 34567–34574.
61. DeWaal, D., Nogueira, V., Terry, A.R., Patra, K.C., Jeon, S.-M., Guzman, G., Au, J., Long, C.P., Antoniewicz, M.R., and Hay, N. (2018). Hexokinase-2 depletion inhibits glycolysis and induces oxidative phosphorylation in hepatocellular carcinoma and sensitizes to metformin. Nat. Commun. *9*, 446.
62. Oliva, M., Muñoz-Aguirre, M., Kim-Hellmuth, S., Wucher, V., Gewirtz, A.D.H., Cotter, D.J., Parsana, P., Kasela, S., Balliu, B., and Viñuela, A. (2020). The impact of sex on gene expression across human tissues. Science *369*, eaba3066.
63. Meister, A. (1988). Glutathione metabolism and its selective modification. J. Biol. Chem. *263*, 17205–17208.
64. Adams, J.D., Lauterburg, B.H., and Mitchell, J.R. (1983). Plasma glutathione and glutathione disulfide in the rat: regulation and response to oxidative stress. J. Pharmacol. Exp. Ther. *227*, 749–754.
65. Jenniskens, F.A., Jopperi-Davis, K.S., Walters, L.C., Schorr, E.N., Rogers, L.K., Welty, S.E., and Smith, C.V. (2002). Effects of fasting on tissue contents of coenzyme A and related intermediates in rats. Pediatr. Res. *52*, 437–442.
66. Lee, M.H., Malloy, C.R., Corbin, I.R., Li, J., and Jin, E.S. (2019). Assessing the pentose phosphate pathway using [2, 3-13C2] glucose. NMR Biomed. *32*, e4096.
67. Bennett, C.F., Kwon, J.J., Chen, C., Russell, J., Acosta, K., Burnaevskiy, N., Crane, M.M., Bitto, A., Vander Wende, H., and Simko, M. (2017). Transaldolase inhibition impairs mitochondrial respiration and induces a starvation-like longevity response in Caenorhabditis elegans. PLoS Genet. *13*, e1006695.
68. Yin, J., Ren, W., Huang, X., Deng, J., Li, T., and Yin, Y. (2018). Potential mechanisms connecting purine metabolism and cancer therapy. Front. Immunol. *9*, 1697.
69. Soñanez-Organis, J.G., Vázquez-Medina, J.P., Zenteno-Savín, T., Aguilar, A., Crocker, D.E., and Ortiz, R.M. (2012). Prolonged fasting increases purine recycling in post-weaned northern elephant seals. J. Exp. Biol. *215*, 1448–1455.
70. Coleman, R.A., and Mashek, D.G. (2011). Mammalian triacylglycerol metabolism: synthesis, lipolysis, and signaling. Chem. Rev. *111*, 6359–6386.
71. Menezes-Filho, S.L., Amigo, I., Luévano-Martínez, L.A., and Kowaltowski, A.J. (2019). Fasting promotes functional changes in liver mitochondria. Biochim. Biophys. Acta Bioenerg. *1860*, 129–135.
72. Cerqueira, F.M., Laurindo, F.R.M., and Kowaltowski, A.J. (2011). Mild mitochondrial uncoupling and calorie restriction increase fasting eNOS, akt and mitochondrial biogenesis. PLoS One *6*, e18433.
73. Graf, M., Hartmann, N., Reichwald, K., and Englert, C. (2013). Absence of replicative senescence in cultured cells from the short-lived killifish Nothobranchius furzeri. Exp. Gerontol. *48*, 17–28. https://doi.org/10.1016/j.exger.2012.02.012.
74. Jones, G.E., and Sargent, P.A. (1974). Mutants of cultured Chinese hamster cells deficient in adenine phosphoribosyl transferase. Cell *2*, 43–54.
75. Sahota, A., Ranjekar, P.K., Alfonzo, J., Lewin, A.S., and Taylor, M.W. (1987). Mutants of Saccharomyces cerevisiae deficient in adenine phosphoribosyltransferase. Mutat. Res. *180*, 81–87.
76. Wang, Y., and Hekimi, S. (2015). Mitochondrial dysfunction and longevity in animals: untangling the knot. Science *350*, 1204–1207.
77. Sun, N., Youle, R.J., and Finkel, T. (2016). The mitochondrial basis of aging. Mol. Cell *61*, 654–666.
78. Tavallaie, M., Voshtani, R., Deng, X., Qiao, Y., Jiang, F., Collman, J.P., and Fu, L. (2020). Moderation of mitochondrial respiration mitigates metabolic syndrome of aging. Proc. Natl. Acad. Sci. USA *117*, 9840–9850.
79. Mohapatra, S., Chakraborty, T., Shimizu, S., Ohta, K., Nagahama, Y., and Ohta, K. (2020). Estrogen and estrogen receptors chauffeur the sex-biased autophagic action in liver. Cell Death Differ. *27*, 3117–3130.
80. Della Torre, S., Mitro, N., Meda, C., Lolli, F., Pedretti, S., Barcella, M., Ottobrini, L., Metzger, D., Caruso, D., and Maggi, A. (2018). Short-term fasting reveals amino acid metabolism as a major sex-discriminating factor in the liver. Cell Metab. *28*, 256–267.e5.
81. Harrison, D.E., Strong, R., Sharp, Z.D., Nelson, J.F., Astle, C.M., Flurkey, K., Nadon, N.L., Wilkinson, J.E., Frenkel, K., Carter, C.S., et al. (2009). Rapamycin fed late in life extends lifespan in genetically heterogeneous mice. Nature *460*, 392–395.
82. Young, G.H., Lin, J.T., Cheng, Y.F., Ho, C.F., Kuok, Q.Y., Hsu, R.C., Liao, W.R., Chen, C.C., and Chen, H.M. (2021). Modulation of adenine phosphoribosyltransferase-mediated salvage pathway to accelerate diabetic wound healing. FASEB J. *35*, e21296.
83. Mauvais-Jarvis, F. (2015). Sex differences in metabolic homeostasis, diabetes, and obesity. Biol. Sex Differ. *6*, 14.
84. Austad, S.N. (2011). Sex differences in longevity and aging. Handb. Biol. Aging, 479–495.
85. Naqvi, S., Godfrey, A.K., Hughes, J.F., Goodheart, M.L., Mitchell, R.N., and Page, D.C. (2019). Conservation, acquisition, and functional impact of sex-biased gene expression in mammals. Science *365*, eaaw7317.
86. Freire, T., Senior, A.M., Perks, R., Pulpitel, T., Clark, X., Brandon, A.E., Wahl, D., Hatchwell, L., Le Couteur, D.G., and Cooney, G.J. (2020). Sex-specific metabolic responses to 6 hours of fasting during the active phase in young mice. J. Physiol. *598*, 2081–2092.
87. Sun, L.Y., Fang, Y., Patki, A., Koopman, J.J.E., Allison, D.B., Hill, C.M., Masternak, M.M., Darcy, J., Wang, J., and McFadden, S. (2017).

Longevity is impacted by growth hormone action during early postnatal period. eLife *6*, e24059.

88. Baar, E.L., Carbajal, K.A., Ong, I.M., and Lamming, D.W. (2016). Sex-and tissue-specific changes in mTOR signaling with age in C57 BL/6J mice. Aging Cell *15*, 155–166.
89. Kanfi, Y., Naiman, S., Amir, G., Peshti, V., Zinman, G., Nahum, L., Bar-Joseph, Z., and Cohen, H.Y. (2012). The sirtuin SIRT6 regulates lifespan in male mice. Nature *483*, 218–221. https://doi.org/10.1038/nature10815.
90. Sharples, A.P., Hughes, D.C., Deane, C.S., Saini, A., Selman, C., and Stewart, C.E. (2015). Longevity and skeletal muscle mass: the role of IGF signalling, the sirtuins, dietary restriction and protein intake. Aging Cell *14*, 511–523.
91. Ashpole, N.M., Logan, S., Yabluchanskiy, A., Mitschelen, M.C., Yan, H., Farley, J.A., Hodges, E.L., Ungvari, Z., Csiszar, A., and Chen, S. (2017). IGF-1 has sexually dimorphic, pleiotropic, and time-dependent effects on healthspan, pathology, and lifespan. GeroScience *39*, 129–145.
92. Pernicova, I., and Korbonits, M. (2014). Metformin—mode of action and clinical implications for diabetes and cancer. Nat. Rev. Endocrinol. *10*, 143–156.
93. Kane, A.E., Sinclair, D.A., Mitchell, J.R., and Mitchell, S.J. (2018). Sex differences in the response to dietary restriction in rodents. Curr. Opin. Physiol. *6*, 28–34.
94. Barzilai, N.R. (2017). Targeting aging with metformin (TAME). Innov. Aging *1*. 743–743.
95. Kulkarni, A.S., Gubbi, S., and Barzilai, N. (2020). Benefits of metformin in attenuating the hallmarks of aging. Cell Metab. *32*, 15–30.
96. Evan, A.P., Bledsoe, S.B., Connors, B.A., Deng, L., Liang, L., Shao, C., Fineberg, N.S., Grynpas, M.D., Stambrook, P.J., and Youzhi, S. (2001). Sequential analysis of kidney stone formation in the Aprt knockout mouse. Kidney Int. *60*, 910–923.
97. Yang, S., and Wang, J. (2015). Estrogen activates AMP-activated protein kinase in human endothelial cells via ERβ/Ca2+/calmodulin-dependent protein kinase kinase β pathway. Cell Biochem. Biophys. *72*, 701–707.
98. Gustavsson, C., Yassin, K., Wahlström, E., Cheung, L., Lindberg, J., Brismar, K., Östenson, C.-G., Norstedt, G., and Tollet-Egnell, P. (2010). Sex-different hepatic glycogen content and glucose output in rats. BMC Biochem. *11*, 38.
99. Guévélou, E., Huvet, A., Galindo-Sánchez, C.E., Milan, M., Quillien, V., Daniel, J.Y., Quéré, C., Boudry, P., and Corporeau, C. (2013). Sex-specific regulation of AMP-activated protein kinase (AMPK) in the Pacific oyster Crassostrea gigas. Biol. Reprod. *89*, 100.
100. Johnson, T.A., Jinnah, H.A., and Kamatani, N. (2019). Shortage of cellular ATP as a cause of diseases and strategies to enhance ATP. Front. Pharmacol. *10*, 98.
101. Murray, A.W. (1971). The biological significance of purine salvage. Annu. Rev. Biochem. *40*, 811–826.
102. Ipata, P.L., Camici, M., Micheli, V., and Tozz, M.G. (2011). Metabolic network of nucleosides in the brain. Curr. Top. Med. Chem. *11*, 909–922.
103. Boitz, J.M., Ullman, B., Jardim, A., and Carter, N.S. (2012). Purine salvage in Leishmania: complex or simple by design? Trends Parasitol. *28*, 345–352.
104. Rajamohan, F., Reyes, A.R., Frisbie, R.K., Hoth, L.R., Sahasrabudhe, P., Magyar, R., Landro, J.A., Withka, J.M., Caspers, N.L., and Calabrese, M.F. (2016). Probing the enzyme kinetics, allosteric modulation and activation of α1-and α2-subunit-containing AMP-activated protein kinase (AMPK) heterotrimeric complexes by pharmacological and physiological activators. Biochem. J. *473*, 581–592.
105. Camici, M., Allegrini, S., and Tozzi, M.G. (2018). Interplay between adenylate metabolizing enzymes and AMP-activated protein kinase. FEBS J. *285*, 3337–3352.
106. Labun, K., Montague, T.G., Krause, M., Torres Cleuren, Y.N., Tjeldnes, H., and Valen, E. (2019). CHOPCHOP v3: expanding the CRISPR web toolbox beyond genome editing. Nucleic Acids Res. *47*, W171–W174.
107. Jao, L.E., Wente, S.R., and Chen, W. (2013). Efficient multiplex biallelic zebrafish genome editing using a CRISPR nuclease system. Proc. Natl. Acad. Sci. USA *110*, 13904–13909. https://doi.org/10.1073/pnas.1308335110.
108. Flurkey, K., Currer, J.M., and Harrison, D.E. (2007). Mouse models in aging research. In The Mouse in Biomedical Research (Elsevier), pp. 637–672.
109. Dodzian, J., Kean, S., Seidel, J., and Valenzano, D.R. (2018). A Protocol for Laboratory Housing of Turquoise killifish (Nothobranchius furzeri). J. Vis. Exp. https://doi.org/10.3791/57073.
110. Salem, M., Bernach, M., Bajdzienko, K., and Giavalisco, P. (2017). A simple fractionated extraction method for the comprehensive analysis of metabolites, lipids, and proteins from a single sample. J. Vis. Exp. https://doi.org/10.3791/55802.
111. Malitsky, S., Ziv, C., Rosenwasser, S., Zheng, S., Schatz, D., Porat, Z., Ben-Dor, S., Aharoni, A., and Vardi, A. (2016). Viral infection of the marine alga Emiliania huxleyi triggers lipidome remodeling and induces the production of highly saturated triacylglycerol. New Phytol. *210*, 88–96.
112. Zheng, L., Cardaci, S., Jerby, L., MacKenzie, E.D., Sciacovelli, M., Johnson, T.I., Gaude, E., King, A., Leach, J.D.G., and Edrada-Ebel, R. (2015). Fumarate induces redox-dependent senescence by modifying glutathione metabolism. Nat. Commun. *6*, 1–12.
113. Lu, Y., Pang, Z., and Xia, J. (2023). Comprehensive investigation of pathway enrichment methods for functional interpretation of LC–MS global metabolomics data. Brief. Bioinform. *24*, bbac553. https://doi.org/10.1093/bib/bbac553.
114. Caspi, R., Billington, R., Keseler, I.M., Kothari, A., Krummenacker, M., Midford, P.E., Ong, W.K., Paley, S., Subhraveti, P., and Karp, P.D. (2020). The MetaCyc database of metabolic pathways and enzymes-a 2019 update. Nucleic Acids Res. *48*, D445–D453.
115. Andrews, S. (2017). FastQC: a Quality Control Tool for High Throughput Sequence Data*2010*.
116. Ewels, P., Magnusson, M., Lundin, S., and Käller, M. (2016). MultiQC: summarize analysis results for multiple tools and samples in a single report. Bioinformatics *32*, 3047–3048.
117. Krueger, F. (2015). Trim Galore. A Wrapper Tool around Cutadapt FastQC to consistently apply quality and adapter trimming to FastQ files. http://www.bioinformatics.babraham.ac.uk/projects/trim_galore/.
118. Martin, M. (2011). Cutadapt removes adapter sequences from high-throughput sequencing reads. EMBnet. J *17*, 10–12.
119. Reichwald, K., Petzold, A., Koch, P., Downie, B.R., Hartmann, N., Pietsch, S., Baumgart, M., Chalopin, D., Felder, M., Bens, M., et al. (2015). Insights into sex chromosome evolution and aging from the genome of a short-lived fish. Cell *163*, 1527–1538. https://doi.org/10.1016/j.cell.2015.10.071.
120. Dobin, A., Davis, C.A., Schlesinger, F., Drenkow, J., Zaleski, C., Jha, S., Batut, P., Chaisson, M., and Gingeras, T.R. (2013). STAR: ultrafast universal RNA-seq aligner. Bioinformatics *29*, 15–21.
121. McCarthy, D.J., Chen, Y., and Smyth, G.K. (2012). Differential expression analysis of multifactor RNA-Seq experiments with respect to biological variation. Nucleic Acids Res. *40*, 4288–4297.
122. Robinson, M.D., McCarthy, D.J., and Smyth, G.K. (2010). edgeR: a Bioconductor package for differential expression analysis of digital gene expression data. Bioinformatics *26*, 139–140.
123. Yu, G., Wang, L.G., Han, Y., and He, Q.Y. (2012). clusterProfiler: an R package for comparing biological themes among gene clusters. OMICS A J. Integr. Biol. *16*, 284–287.
124. Carlson, M., Falcon, S., Pages, H., and Li, N. (2019). org. Hs. eg. db: genome wide annotation for human. R Package version *3*, 265.
125. Pagès, H., Carlson, M., Falcon, S., and Li, N. (2023). AnnotationDbi: manipulation of SQLite-based annotations in bioconductor R Package Version1. https://doi.org/10.18129/B9.bioc.AnnotationDbi.

126. Gu, Z., Eils, R., and Schlesner, M. (2016). Complex heatmaps reveal patterns and correlations in multidimensional genomic data. Bioinformatics *32*, 2847–2849.

127. Harel, I., Chen, Y.R., Ziv, I., Singh, P.P., Negredo, P.N., Goshtchevsky, U., Wang, W., Astre, G., Moses, E., and McKay, A. (2022). Identification of protein aggregates in the aging vertebrate brain with prion-like and phase separation properties. https://doi.org/10.1101/2022.02.26.482115.

128. Harel, I., Maezawa, Y., Avraham, R., Rinon, A., Ma, H.Y., Cross, J.W., Leviatan, N., Hegesh, J., Roy, A., Jacob-Hirsch, J., et al. (2012). Pharyngeal mesoderm regulatory network controls cardiac and head muscle morphogenesis. Proc. Natl. Acad. Sci. USA *109*, 18839–18844. https://doi.org/10.1073/pnas.1208690109.

129. Theis, S., Patel, K., Valasek, P., Otto, A., Pu, Q., Harel, I., Tzahor, E., Tajbakhsh, S., Christ, B., and Huang, R. (2010). The occipital lateral plate mesoderm is a novel source for vertebrate neck musculature. Development *137*, 2961–2971.

130. Nathan, E., Monovich, A., Tirosh-Finkel, L., Harrelson, Z., Rousso, T., Rinon, A., Harel, I., Evans, S.M., and Tzahor, E. (2008). The contribution of Islet1-expressing splanchnic mesoderm cells to distinct branchiomeric muscles reveals significant heterogeneity in head muscle development. Development *135*, 647–657.

131. Harel, I., Nathan, E., Tirosh-Finkel, L., Zigdon, H., Guimarães-Camboa, N., Evans, S.M., and Tzahor, E. (2009). Distinct origins and genetic programs of head muscle satellite cells. Dev. Cell *16*, 822–832.

132. Van Keymeulen, A., Mascre, G., Youseff, K.K., Harel, I., Michaux, C., De Geest, N., Szpalski, C., Achouri, Y., Bloch, W., Hassan, B.A., et al. (2009). Epidermal progenitors give rise to Merkel cells during embryonic development and adult homeostasis. J. Cell Biol. *187*, 91–100.

133. Harel, I., and Tzahor, E. (2012). Head muscle development. In Craniofacial Muscles (Springer), pp. 11–28.

134. Gruenbaum-Cohen, Y., Harel, I., Umansky, K.-B., Tzahor, E., Snapper, S.B., Shilo, B.-Z., and Schejter, E.D. (2012). The actin regulator N-WASp is required for muscle-cell fusion in mice. Proc. Natl. Acad. Sci. USA *109*, 11211–11216.

135. Motamedi, M., Shamsaldini, F., Teimori, A., and Hesni, M.A. (2019). Histomicroscopy and normal anatomy of the adult killifish Aphanius hormuzensis (Teleostei; Aphaniidae) from the Persian Gulf coastal environment. Microsc. Res. Tech. *82*, 466–480. https://doi.org/10.1002/jemt.23190.

136. Humphrey, J.D. (2007). Systemic pathology of fish: a text and atlas of normal tissues in teleosts and their response in disease. J. Fish Diseases *30*, 381–382.

137. Di Cicco, E., Tozzini, E.T., Rossi, G., and Cellerino, A. (2011). The short-lived annual fish Nothobranchius furzeri shows a typical teleost aging process reinforced by high incidence of age-dependent neoplasias. Exp. Gerontol. *46*, 249–256. https://doi.org/10.1016/j.exger.2010.10.011.

138. Feist, S.W., Stentiford, G.D., Kent, M.L., Ribeiro Santos, A.R., and Lorance, P. (2015). Histopathological assessment of liver and gonad pathology in continental slope fish from the northeast Atlantic Ocean. Mar. Environ. Res. *106*, 42–50.

139. Sternberg, S.S. (1992). Histology for pathologists. Serous Membr. *1992*, 499–514.

140. Griffett, K., Solt, L.A., El-Gendy, B.E.-D.M., Kamenecka, T.M., and Burris, T.P. (2013). A liver-selective LXR inverse agonist that suppresses hepatic steatosis. ACS Chem. Biol. *8*, 559–567.

141. Parafati, M., Kirby, R.J., Khorasanizadeh, S., Rastinejad, F., and Malany, S. (2018). A nonalcoholic fatty liver disease model in human induced pluripotent stem cell-derived hepatocytes, created by endoplasmic reticulum stress-induced steatosis. Dis. Model. Mech. *11*, dmm033530.

142. Žák, J., Dyková, I., and Reichard, M. (2020). Good performance of turquoise killifish (Nothobranchius furzeri) on pelleted diet as a step towards husbandry standardization. Sci. Rep. *10*, 8986. https://doi.org/10.1038/s41598-020-65930-0.

143. Landgraf, K., Schuster, S., Meusel, A., Garten, A., Riemer, T., Schleinitz, D., Kiess, W., and Körner, A. (2017). Short-term overfeeding of zebrafish with normal or high-fat diet as a model for the development of metabolically healthy versus unhealthy obesity. BMC Physiol. *17*, 4.

144. Lane, M.A., Ingram, D.K., and Roth, G.S. (1998). 2-deoxy-D-glucose feeding in rats mimics physiologic effects of calorie restriction. J. Anti-Aging Med. *1*, 327–337.

145. Gonzalez, A.A., Kumar, R., Mulligan, J.D., Davis, A.J., Weindruch, R., and Saupe, K.W. (2004). Metabolic adaptations to fasting and chronic caloric restriction in heart, muscle, and liver do not include changes in AMPK activity. Am. J. Physiol. Metab. *287*, E1032–E1037.

146. Wijngaarden, M.A., van der Zon, G.C., van Dijk, K.W., Pijl, H., and Guigas, B. (2013). Effects of prolonged fasting on AMPK signaling, gene expression, and mitochondrial respiratory chain content in skeletal muscle from lean and obese individuals. Am. J. Physiol. Endocrinol. Metab. *304*, E1012–E1021.

147. Cakmak, G., Togan, I., and Severcan, F. (2006). 17β-estradiol induced compositional, structural and functional changes in rainbow trout liver, revealed by FT-IR spectroscopy: a comparative study with nonylphenol. Aquat. Toxicol. *77*, 53–63.

148. Schindelin, J., Arganda-Carreras, I., Frise, E., Kaynig, V., Longair, M., Pietzsch, T., Preibisch, S., Rueden, C., Saalfeld, S., Schmid, B., et al. (2012). Fiji: an open-source platform for biological-image analysis. Nat. Methods *9*, 676–682.

149. Mackay, G.M., Zheng, L., Van Den Broek, N.J.F., and Gottlieb, E. (2015). Analysis of cell metabolism using LC-MS and isotope tracers. Methods Enzymol. *561*, 171–196.

150. Pietzke, M., and Vazquez, A. (2020). Metabolite AutoPlotter-an application to process and visualise metabolite data in the web browser. Cancer Metab. *8*, 15.

151. Hartmann, N., Reichwald, K., Wittig, I., Dröse, S., Schmeisser, S., Lück, C., Hahn, C., Graf, M., Gausmann, U., Terzibasi, E., et al. (2011). Mitochondrial DNA copy number and function decrease with age in the short-lived fish Nothobranchius furzeri. Aging Cell *10*, 824–831. https://doi.org/10.1111/j.1474-9726.2011.00723.x.

152. Eisenberg, E., and Levanon, E.Y. (2018). A-to-I RNA editing—immune protector and transcriptome diversifier. Nat. Rev. Genet. *19*, 473–490.

153. Schmieder, R., and Edwards, R. (2011). Quality control and preprocessing of metagenomic datasets. Bioinformatics *27*, 863–864.

154. Bolger, A.M., Lohse, M., and Usadel, B. (2014). Trimmomatic: a flexible trimmer for Illumina sequence data. Bioinformatics *30*, 2114–2120.

155. Chen, N. (2004). Using Repeat Masker to identify repetitive elements in genomic sequences. Curr. Protoc. Bioinform. *5*, 4–10.

156. Ou, S., Su, W., Liao, Y., Chougule, K., Agda, J.R.A., Hellinga, A.J., Lugo, C.S.B., Elliott, T.A., Ware, D., and Peterson, T. (2019). Benchmarking transposable element annotation methods for creation of a streamlined, comprehensive pipeline. Genome Biol. *20*, 1–18.

157. Porath, H.T., Carmi, S., and Levanon, E.Y. (2014). A genome-wide map of hyper-edited RNA reveals numerous new sites. Nat. Commun. *5*, 4726.

158. Buchumenski, I., Holler, K., Appelbaum, L., Eisenberg, E., Junker, J.P., and Levanon, E.Y. (2021). Systematic identification of A-to-I RNA editing in zebrafish development and adult organs. Nucleic Acids Res. *49*, 4325–4337.

159. Roth, S.H., Levanon, E.Y., and Eisenberg, E. (2019). Genome-wide quantification of ADAR adenosine-to-inosine RNA editing activity. Nat. Methods *16*, 1131–1138.

160. Patro, R., Duggal, G., Love, M.I., Irizarry, R.A., and Kingsford, C. (2017). Salmon provides fast and bias-aware quantification of transcript expression. Nat. Methods *14*, 417–419.

161. Li, H., and Durbin, R. (2009). Fast and accurate short read alignment with Burrows–Wheeler transform. Bioinformatics *25*, 1754–1760.

## STAR★METHODS

### KEY RESOURCES TABLE

| REAGENT or RESOURCE | SOURCE | IDENTIFIER |
|---|---|---|
| Antibodies | | |
| Anti-Phospho-Acetyl-CoA Carboxylase (Ser79) Antibody | Cell Signaling Technology | CST-3661 |
| Anti-Acetyl-CoA Carboxylase (C83B10) Rabbit mAb | Cell Signaling Technology | CST-3676 |
| Anti-S6 Ribosomal Protein (5G10) Rabbit mAb | Cell Signaling Technology | CST-2217 |
| Anti-Phospho-S6 Ribosomal Protein (Ser235/236) | Cell Signaling Technology | CST-2211 |
| Anti-AMPKα (D5A2) Rabbit mAb | Cell Signaling Technology | CST-5831 |
| Anti-Phospho-AMPKα (Thr172) (40H9) Rabbit mAb | Cell Signaling Technology | CST-2535 |
| Mouse anti-actin monoclonal clone C4 | MP Biomedicals | 0869100; RRID: AB_2920628 |
| Goat Anti-Rabbit IgG H&L (HRP) | Abcam | ab6721; RRID: AB_955447 |
| Goat Anti-Mouse IgG H&L (HRP) | Abcam | ab6789; RRID: AB_955439 |
| Chemicals, Peptides, and Recombinant Proteins | | |
| Hoechst 33342 Solution (20 mM) | Thermo Scientific™ | 62249 |
| BODIPY® 493/503/10mg | Invitrogen™ | D3922 |
| PFA 16% solution EM GRADE | Electron Microscopy Sciences | 15710 |
| Leibovitz's L-15 Medium, GlutaMAX™ Supplement | Gibco™ | 31415086 |
| MitoView™ 633 | Biotium | 70055 |
| Gentamicin (50 mg/mL) | Gibco™ | 15750060 |
| Penicillin/Streptomycin 10,000 U\ml | Gibco™ | 15140122 |
| Primocin™ | Invitrogen™ | ant-pm |
| Trypsin-EDTA (0.25%), phenol red | Gibco™ | 25200056 |
| Fetal Bovine Serum (FBS) | Gibco™ | 10270106 |
| Dulbecco's Phosphate Buffered Saline (DPBS) | Biological Industries | 02-023-1A |
| Collagenase Type P | Merck Millipore | 11213857001 |
| Dispase II protease | Sigma Aldrich | D4693 |
| Phosphatase Inhibitor Cocktail (2 Tubes, 100X) | Biotool | B15001 |
| Protease Inhibitor Cocktail (EDTA-Free, 100X in DMSO) | Biotool | B14001 |
| PageRuler™ Plus Prestained Protein Ladder, 10-250 kDa | Thermo Scientific™ | 26619 |
| EZ-ECL KIT | Biological Industries | 20-500 |
| TRIS HCl | Sigma Aldrich | 10812846001 |
| Glycerol anhydrous AR | Bio-Lab | CAT No 000712050100 |
| 2-Mercaptoethanol | Sigma Aldrich | M3148 |
| Bromophenol Blue | Sigma Aldrich | 114391 |
| Invitrogen Novex Tris Glycine SDS Running Buffer (10X) | Thermo Scientific™ | LC2675 |
| Bovine Serum Albumin,heat shock fraction, pH 7, ≥ 98% | Sigma Aldrich | A7906 |
| Adenine, BioReagent suitable for cell culture, | Sigma Aldrich | A2786 |

(*Continued on next page*)

*Continued*

| REAGENT or RESOURCE | SOURCE | IDENTIFIER |
|---|---|---|
| Beta-Estradiol, 99% (dry wt.), ca 3% water | Holland Moran | L03801 |
| 8-Azaadenine 97% (CAS 1123-54-2) | Holland Moran | HC003NHH |
| Ethyl 3-aminobenzoate methanesulfonate salt (Tricaine) | Sigma Aldrich | A5040 |
| Ponceau S solution | Sigma Aldrich | P7170 |
| TRI Reagent® | Sigma Aldrich | T9424 |
| **Software and Algorithms** | | |
| GraphPad Prism (version 7 for Windows) | GraphPad software | https://www.graphpad.com/ |
| Fiji 1.53c (plus) | NIH | https://imagej.net/Fiji |
| Matlab R2021a | The MathWorks, Inc. | https://www.mathworks.com/ |
| FlowView confocal software | Olympus, Japan | N/A |
| Olympus cellSens Dimension 3.1 | Olympus | N/A |
| FastQC | Andrews[115] | Version 0.11.8 |
| fastx-toolkits | N/A | Version 0.0.13 |
| Trim Galore! | Krueger[117] | Version 0.6.4 |
| Cutadapt | Martin[118] | Version 3.4 |
| STAR | Dobin et al.[120] | Version 2.7.6a |
| edgeR | McCarthy et al.[121]; Robinson et al.[122] | Version 3.32.1 |
| clusterProfiler | Yu et al.[123] | Version 3.18.1 |
| GSVA | Hänzelmann et al.[51] | Version 1.40.1 |
| Trimmomatic | Bolger et al.[154] | Version 0.39 |
| RepeatMasker | Chen[155] | Version 4.1.0 |
| EDTA | Ou et al.[156] | Version 1.9.6 |
| RNA Editing Indexer | https://github.com/a2iEditing/RNAEditingIndexer | N/A |
| Salmon | Patro et al.[160] | Version 1.4 |
| BWA | Li and Durbin[161] | Version 0.7.17 |
| **Critical commercial assays** | | |
| Seahorse XFp FluxPak | Agilent Technologies | 103022-100 |
| Seahorse XFp Cell Mito Stress Kit | Agilent Technologies | 103010-100 |
| Seahorse XF Glycolysis Stress Kit | Agilent Technologies | 103017-100 |
| Novex™ WedgeWell™ 4 to 20%, Tris-Glycine, 1.0 mm, Mini Protein Gel, 15-well | Invitrogen™ | XP04205BOX |
| Verso cDNA Synthesis Kit | Thermo Scientific™ | AB1453 |
| Pierce™ BCA Protein Assay Kit | Thermo Scientific™ | 23225 |
| Fast SYBR™ Green Master Mix | Applied Biosystems™ | 4385612 |
| Direct-Zol RNA Miniprep | Zymo | ZR-R2050 |
| QIAamp DNA Micro Kit | Qiagen | 56304 |
| Kapa RNA HyperPrep | ROCHE | 08105936001 |
| NextSeq 500/550 High Output Kit v2.5 (75 Cycles) | Illumina | 20024906 |
| **Deposited data** | | |
| RNA sequencing, raw data | This paper | GEO: GSE190757 |
| RNA sequencing, analysis | This paper | https://doi.org/10.5281/zenodo.7961783 |
| **Oligonucleotides** | | |
| CDKN2A/B-qPCR_F | Hartmann et al.[151] | N/A |
| CDKN2A/B-qPCR_R | Hartmann et al.[151] | N/A |

(*Continued on next page*)

| Continued | | |
|---|---|---|
| REAGENT or RESOURCE | SOURCE | IDENTIFIER |
| 16S rRNA-qPCR_F | Hartmann et al.[151] | N/A |
| 16S rRNA-qPCR_R | Hartmann et al.[151] | N/A |
| Universal reverse oligonucleotide: 5'-AAAAGCACCGACTCGGTGCC ACTTTTTCAAGTTGATAACGGAC TAGCCTTATTTTAACTTGCTATTT CTAGCTCTAAAAC-3' (Used for all gRNA templates) | Rozenberg et al.[47] | N/A |
| Variable oligonucleotide: 5'- TAATACGACTCACTATA[GG-(N) 18]GTTTTAGAGCTAGA AATAGCAAG-3' (gRNA target sequence in bold, and unique for each gRNA) | Rozenberg et al.[47] | N/A |
| APRT gRNA (Variable oligo) 5'-TAATACGACTCACTATAGGGGTC CAAACAGGAAGCCAGTTTTAGAGCT AGAAATAGCAAG-3' | This paper | APRT-gRNA2 |
| Fish | | |
| African turquoise killifish, GRZ strain (*Nothobranchius furzeri*) | This paper | N/A |
| Killifish APRT$^{\Delta 8}$ CRISPR mutants | This paper | N/A |

## RESOURCE AVAILABILITY

### Lead contact

Further information and requests for resources and reagents should be directed to and will be fulfilled by the lead contact, Itamar Harel (itamarh@mail.huji.ac.il).

### Materials availability

The APRT fish line generate in this study is available upon request.

### Data and code availability

All raw RNA sequencing data, as well as processed datasets could be found in the Gene Expression Omnibus database, under accession number GEO: GSE190757. All Lipidomic and metabolomic datasets could be found in Table S3. The codes and results supporting the current study are available in the GitHub repository for this paper https://github.com/Harel-lab/APRT-sex-differences. Any additional information required to reanalyze the data reported in this paper is available from the lead contact upon request.

## EXPERIMENTAL MODEL AND SUBJECT DETAILS

### African turquoise killifish strain, husbandry, and maintenance

The African turquoise killifish (GRZ strain) were housed as previously described.[42,44] Fish were housed at 28°C in a central filtration recirculating system with a 12 h light/dark cycle at the Hebrew University of Jerusalem (Aquazone ltd, Israel). Until the age of 2 weeks, fish were exclusively fed with live Artemia (#109448, Primo). Starting week 3, fish were fed three times a day on weekdays (and once a day on weekends), with GEMMA Micro 300 Fish Diet (Skretting Zebrafish, USA), supplemented with Artemia twice a day. In these conditions, killifish lifespan was approximately 4-6 months. The APRT loss-of-function allele was maintained as heterozygous and propagated by crossing with WT fish. All turquoise killifish care and uses were approved by the Subcommittee on Research Animal Care at the Hebrew University of Jerusalem (IACUC protocol #NS-18-15397-2).

### CRISPR/Cas9 target prediction and gRNA synthesis

CRISPR/Cas9 genome-editing protocols were performed according to Astre et al.[44] In brief, for targeting APRT, conserved regions that were upstream of functional or active protein domains were selected. gRNA target sites were identified using CHOPCHOP (https://chopchop.rc.fas.harvard.edu/),[106] and were as follows (PAM sites are in bold): APRT Exon 3: 5′- GGGGTCCAAACAG GAAGCCA**CGG**-3′. Design and hybridization of variable oligonucleotides (which are gRNA-specific) with a universal reverse oligonucleotide was performed according to Astre et al.,[44] and the resulting products were used as a template for *in vitro* transcription.

gRNAs were *in vitro* transcribed and purified using the MAXIscript T7 kit (ThermoFisher # AM1312), according to the manufacturer's protocol.

### Production of Cas9 mRNA

Experiments were performed according to Astre et al.[44] The pCS2-nCas9n expression vector was used to produce Cas9 mRNA (Addgene, #47929).[107] Capped and polyadenylated Cas9 mRNA was *in vitro* transcribed and purified using the mMESSAGE mMACHINE SP6 ULTRA (ThermoFisher # AM1340).

### Microinjection of turquoise killifish embryos and generation of mutant fish using CRISPR/Cas9

Microinjection of turquoise killifish embryos was performed according to Astre et al.[44] Briefly, nCas9n-encoding mRNA (300 ng/μL) and gRNA (30 ng/μL) were mixed with phenol-red (P0290, Sigma-Aldrich) and co-injected into one-cell stage fish embryos. Sanger DNA sequencing was used for detecting successful germline transmission on F1 embryos. The genomic area encompassing the targeted site (~600 bp) was PCR-amplified using the following primer sequences: APRT_F: 5'-TTCCCTCTTTACTGACGTCTCA-3' and APRT_R: 5'-GAAAAATTCCCACAGTAAGAATGAA-3'. Fish with desired alleles were maintained as stable lines and further outcrossed to minimize potential off-target effects.

### Generation of primary fibroblast cultures from killifish tail fins

Adult fish (8-12 weeks old), of the indicated genotype and gender were sedated with MS-222 (200 mg/L Tricaine, in system water). All following experiments were conducted at 28°C unless stated otherwise. Following sedation, a 2–3 mm tissue was trimmed from the tail fin using a sterile razor blade, and individually disinfected for 10 min with a 25 ppm iodine solution (PVP-I, Holland Moran 229471000) in DPBS (Biological Industries). Followed by a rinse with DPBS, tissue samples were incubated for 2 h with 1 mL of an antibiotic solution containing Gentamicin (50 μg/mL Gibco) and Primocin™ (50 μg/mL, InvivoGen) in DPBS at room temperature. Tissues were then transferred into an enzymatic digestion buffer (200 μL, in a 24-well plate) containing Dispase II (2 mg/mL, Sigma Aldrich) and Collagenase Type P (0.4 mg/mL, Merck Millipore) in Leibovitz's L-15 Medium (Gibco), and mechanical dissociation was applied with a sterile pair of scissors. Crudely dissociated tissue was incubated in the enzymatic digestion buffer for 15 min. The digested tissue was then mixed with 400 μL of complete Leibovitz's L-15 growth medium (Gibco), supplemented with Fetal Bovine Serum (15% FBS, Gibco), penicillin/streptomycin (50 U/ml, Gibco), Gentamicin (Gibco, 50 μg/ml) and Primocin™ (50 μg/ml, InvivoGen), and incubated overnight for continued mild digestion. The day after, the digested tissue was homogenized with a 1 mL pipette, transferred into a 1.5 ml Eppendorf tube, and centrifuged at 200 g for 10 min at 28°C. Supernatant was carefully removed, the cell pellet was resuspended in 1 mL of growth medium, and plated in a 24-well plate. During the first 7 days, cells were washed daily with fresh media before adding new media. When cells reached 85–90% confluency, they were passaged with Trypsin-EDTA 0.05% (0.25% Trypsin-EDTA, diluted in DPBS). Cells were incubated at 28°C humidified incubator (Binder, Thermo Scientific) with normal air composition, and were used for downstream applications between passages 4-12.

## METHOD DETAILS

### Organ isolation

Age groups were selected according to classical guidelines for young and old mice[108] and fish,[44,109] relative to the maturity and median lifespan at our husbandry conditions. Individual killifish, according to the specified age, gender, genotype, and feeding condition, were euthanized in 400 mg/L of Tricaine in system water. Animals were dissected on ice under a binocular stereo microscope (Leica S9E) according to Astre et al.[44] Whole livers or muscles were harvested, cut in half, and placed in two separate tubes. For each fish, the organs were processed for metabolomic and lipidomic profiling, and/or for RNA sequencing (see below). Following weight measurements, tubes were snap-frozen in liquid nitrogen, and stored in -80°C until all samples were collected. All samples were collected during the morning time, between 9 am to 12 pm, to reduce the potential confounding effects driven by circadian rhythms.

### Lipid and polar metabolic profiling

#### *Sample preparation*

Extraction and analysis of lipids and polar metabolites was performed at the Life Sciences Core Facilities, Metabolic Profiling Unit (Weizmann Institute of Science), as previously described in Salem et al.[110] and Malitsky et al.[111] with some modifications. Briefly, liver samples were lyophilized, ground to powder and mixed with 1 mL of a pre-cooled (−20°C) homogenous methanol:methyl-tert-butyl-ether (MTBE) 1:3 (v/v) mixture, containing the following internal standards: 0.1 μg/mL of Phosphatidylcholine (17:0/17:0) (Avanti), 0.4 μg/mL of Phosphatidylethanolamine (17:0/17:0, 0.15 nmol/mL of Ceramide/Sphingoid Internal Standard Mixture I (Avanti, LM6005), 0.0267 μg/mL d5-TG Internal Standard Mixture I (Avanti, LM6000) and 0.1 μg/mL Palmitic acid-13C (Sigma, 605573). The tubes were vortexed and then sonicated for 30 min in ice-cold Transsonic 460/H sonication bath (Elma) at 35 kHz (taken for a brief vortex every 10 min). Then, UPLC-grade water: methanol (3:1, v/v) solution (0.5 mL), containing internal polar metabolite standards (C13 and N15 labeled amino acids standard mix, Sigma, 767964) were added to the tubes. Following 5 min centrifugation at maximum speed, the upper organic phase was transferred into 2 mL Eppendorf tube. The polar phase was re-extracted as

described above, with 0.5 mL of MTBE. Both parts of organic phase were combined and dried (at 21°C setting) using a Refrigerated CentriVap Concentrator (Labconco) and then stored at −80°C until analysis. Lower, polar phase, was similarly lyophilized and stored at −80°C until analysis.

### LC-MS for lipidomic analysis

For analysis, the dried lipid extracts were re-suspended in 150 μL mobile phase B (see below) and centrifuged again at maximum speed at 4°C for 5 min. Lipid extracts were analyzed using a Waters ACQUITY I class UPLC system coupled to a mass spectrometer (Thermo Exactive Plus Orbitrap) which was operated in switching positive and negative ionization mode. The analysis was performed using Acquity UPLC System combined with chromatographic conditions as described in Malitsky et al.[111] with small alterations. Briefly, the chromatographic separation was performed on an ACQUITY UPLC BEH C8 column (2.1×100 mm, i.d., 1.7 μm) (Waters Corp., MA, USA). The mobile phase A consisted of 45% water (UPLC grade) with 1% 1 M NH4Ac, 0.1% acetic acid, and of 55% mobile phase B (acetonitrile: isopropanol (7:3) with 1% 1 M NH4Ac, 0.1% acetic acid). The column was maintained at 40°C and flow rate of mobile phase was 0.4 mL/min. Mobile phase A was run for 1 min at 100%, then it was gradually reduced to 25% at 12 min, following a gradual decrease to 0% at 16 min. Then, mobile phase B was run at 100% until 21 min, and mobile phase A was set to 100% at 21.5 min. Finally, the column was equilibrated at 100% A until 25 min.

### Lipid identification and quantification

Orbitrap data was analyzed using LipidSearch™ software (Thermo Fisher Scientific). The validation of the putative identification of lipids was performed by comparing to home-made library which contains lipids produced by various organisms and on the correlation between retention time (RT), carbon chain length, and degree of unsaturation. Relative levels of lipids were normalized to the internal standards and the amount of tissue used for analysis.

### LC-MS for polar metabolite analysis

For metabolic profiling of the polar phase samples, the lyophilized pellets were dissolved using 150 μL DDW-methanol (1:1), centrifuged twice (at maximum speed) to remove possible precipitants, and were injected into the LC-MS system. Metabolic profiling of the polar phase was performed as described in Zheng et al.[112] with minor modifications described below. Briefly, analysis was performed using Acquity I class UPLC System combined with mass spectrometer (Thermo Exactive Plus Orbitrap) which was operated in a negative ionization mode. The LC separation was performed using the SeQuant Zic-pHilic (150 mm × 2.1 mm) with the SeQuant guard column (20 mm × 2.1 mm) (Merck). The Mobile phase B was acetonitrile; Mobile phase A consisted of 20 mM ammonium carbonate with 0.1% ammonia hydroxide in water:acetonitrile (80:20, v/v). The flow rate was kept at 200 μL/min and gradient as follows: 0-2 min 75% of B, 17 min 12.5% of B, 17.1 min 25% of B, 19 min 25% of B, 19.1 min 75% of B, 23 min 75% of B.

### Polar metabolites identification and quantification

The data processing was performed using TraceFinder™ 4 software (Thermo Fisher) and compounds were identified by accurate mass, retention time, isotope pattern, fragments, and verified using in-house mass spectra library.

### Mass spectrometry analysis

Samples were normalized by internal standard and sample weight. Metabolites and lipids were omitted if they were detected in less than 70% of the samples (19/27 samples), with a final list of 140 metabolites and 787 lipids. Values were $\log_2$ transformed and normalized by the average of each metabolite or lipid. Hierarchical clustering was based on Pearson correlation. MetaboAnalyst confirmed the normality of the data.[113]

To perform statistical analysis for both metabolomics and lipidomics data, we used two-sided unpaired t-test between the WT and *APRT*$^{\Delta 8/+}$ in each experimental condition (age and feeding, i.e. #1 vs. #2, #3 vs. #4 etc.) and FDR correction. Metabolomics: we used BioCyc[114] to classify the metabolites into pathways. We focused on energy pathways and presented the top metabolites from the ranked list (ranked according to t-test between group #7 and #8). In the heatmap, we presented the top 5-7 metabolites. Lipidomics: data was classified according to specific lipid species.

## RNA sequencing

### RNA-seq library preparation

Organs were isolated as described above. Samples were disrupted by bead beating in 300 μl of TriZol (Sigma) and a single 3 mm metal bead (Eldan, BL6693003000) using TissueLyzer LT (QIAGEN, #85600) with a dedicated adaptor (QIAGEN, #69980). Beating was performed twice at 50 Hz for 2 min. RNA extraction was performed with Direct-zol RNA Purification Kits (Zymo). RNA concentration and quality were determined by using an Agilent 2100 bioanalyser (Agilent Technologies). For liver samples, library preparation was performed using KAPA mRNA HyperPrep Kit (ROCHE-08105936001) according to the recommended protocols. Library concentrations were measured by Qubit (dsDNA HS, Q32854), and quality was measured by Tape Station (HS, 5067-5584). Libraries were sequenced by NextSeq 500 high output kit V2 75 cycle, 75 bp single-end (Illumina, 20024906), with ~30 million reads per sample. For muscle samples, library preparation was performed using KAPA Stranded mRNA-Seq Kit (ROCHE-07962193001) according to the recommended protocols. Library quantity and pooling were measured by Qubit (dsDNA HS, Q32854), Size selection at 4% agarose gel. Library quality was measured by Tape Station (HS, 5067-5584). Libraries were sequenced by NextSeq 2000 P3, 50 cycle, 70 bp single-end (Illumina, 20046810) with ~35 million reads per sample.

### RNA sequencing analysis

Quality control and adapter trimming of the fastq sequence files were performed with FastQC (v0.11.8),[115] multiQC (v1.12),[116] fastx-toolkits (v0.0.13), Trim Galore! (v0.6.4),[117] and Cutadapt (v3.4).[118] Options were set to remove Illumina TruSeq adapters and end sequences to retain high-quality bases with *phred* score > 20 and a remaining length > 20 bp. Successful processing was verified

by re-running FastQC. Reads was mapped and quantified to the killifish genome Nfu_20140520[41,119] using STAR 2.7.6a.[120] The liver and muscle samples were analyzed separately. Differential gene expression as a function of age, genotype, and the interaction between age and genotype, or the interaction between age and sex was performed using the edgeR package (v3.32.1),[121,122] and the exact design details of each analysis are described on the main text. One sample (sample #35, liver) did not pass the quality control because of high number of short unmapped reads. However, analysis with or without that sample gave rise to overall similar results. Therefor we decided not to remove this sample from our analysis. In the liver analysis, the three main experimental conditions (males fully fed, males fasted, and female fasted) were sequenced separately. Therefore, analysis was performed on each dataset independently, for increased robustness. However, the muscle samples were sequenced together to allow direct compared between sexes.

#### *Gene ontology enrichment analysis*

Enriched Gene Ontology (GO) terms associated with transcripts levels (from either old versus young, heterozygous versus WT, genotype-age interaction analysis, or age-sex interaction) were identified using Gene Set Enrichment Analysis (GSEA) implemented in R package clusterProfiler (v3.18.1).[123] All the transcripts were ranked and sorted in descending order based on multiplication of $log_2$ transformed fold change and -$log_{10}$(FDR). Note that due to random seeding effect in GSEA, the exact p-value and rank of the enriched terms may differ for each run. These random seeds did not qualitatively affect the enrichment analyses. GO terms were based on human GO annotations from org.Hs.eg.db (v3.13.0)[124] and AnnotationDbi (v1.54.1).[125] Heatmap visualization was perform using ComplexHeatmap (v2.8.0)[126] with hierarchical clustering using Pearson correlation. Gene Set Variance Analysis (GSVA) was performed using GSVA R package (v1.40.1).[51] Gene sets were selected according to GO term or Reactome Pathway Databases. The gene-by-sample matrix was converted to gene-set-by-sample matrix, and the GSVA score was calculated for gene sets with a minimum of 5 detected genes. Data visualization was performed using heatmap as describe above.

#### *Principal component analysis (PCA)*

Standardized $log_2$ transformed normalized count per million (CPM) were used as input for principal component analysis (PCA). PCA was performed using autoplot function implemented in R package ggfortify (v0.4.12) and plotted using ggplot2 (v3.3.5).

#### *Comparing transcriptional longevity interventions between killifish and mice*

The transcriptional signature of 8 longevity intervention was obtained from a previously published comprehensive data-set in mouse liver.[55] The transcriptional signature of the *APRT* mutation in killifish was obtained by comparing WT and *APRT*$^{\Delta 8/+}$ mutants (fully-fed, old male livers). We appliedthe same enrichment strategy described in Tyshkovskiy et al.,[55] using GSEA and msigdbr R package (v7.5.1). We visualized all enriched pathways using the normalized enrichment score by a heatmap (as describe above), in both mice and killifish,

### Survival, maturity, and growth assays

#### *Lifespan measurements*

For reproducible lifespan experiments, constant housing parameters are very important.[44,109] Following hatching, fish were raised with a following density control: 10 fish in a 1-liter tank for week 1, 5 fish in a 3-liter tank for weeks 2-4. From this point onwards, adult fish were genotyped and single housed in a 1-liter tanks for their remaining lifespan. Plastic plants were added for enrichment. Both male and female fish were used for lifespan experiments, and were treated identically. Fish mortality was documented daily starting week 4. Lifespan analyses were performed using GraphPad Prism for all survival curves with a Kaplan-Meier estimator. To compare the survival curves between different experimental groups, we performed log rank test to examine if the survival curves are significantly different.

#### *Maturity and growth measurements*

As fish had to be independently evaluated prior to genotyping, housing was slightly different from lifespan experiments, and fish were individually housed in a 1-liter tank starting week 2. For sexual maturity assay (in males only) coloration status of the fish was visually scored according to the onset of tail coloration. For measuring growth, fish were imaged at the indicated timepoints with a Canon Digital camera EOS 250D, prime lens Canon EF 40 mm f/2.8 STM that documented body length. To limit vertical movement during imaging, fish were positioned in a water tank with 3 cm water depth, and images were taken from the top using fixed lighting and height. A ruler was included in each image for accurate scale. Body length was then calculated (using Matlab R2021a), by converting pixel number to centimeters using the included reference ruler.

### Fertility analysis

Fish fertility was evaluated according to Harel et al.[43] Briefly, 5 independent pairs of fish of the indicated genotypes were placed in the same tank, each consisting of one male and one age-matched female. All breeding pairs were allowed to continuously breed on sand trays, and embryos were collected and counted on a weekly basis for 4 weeks. Unfertilized eggs are easily identified, as they die shortly after egg-laying and the yolk becomes opaque. Results were expressed as a ratio of fertilized eggs per week of egg-lay. The 4-week average of eggs collected for each mating pair was considered as one data point. Significance was calculated using unpaired parametric t test in Prism (GraphPad).

### Histology

Tissues samples were processed according to previous reports.[37,38,41–45,56,127–134] For paraffine sections, the body cavity of the fish was opened, and following a 72 h fixation in 4% PFA solution at 4°C, samples were embedded in either paraffin or 2- hydroxyethyl methacrylate (Electron microscopy Sciences). Sections of 3-6 μm were stained with hematoxylin and eosin and examined by

microscopy. For cryosections, isolated livers were incubated overnight in 4% PFA at 4°C, and then placed in 30% sucrose in DPBS at 4°C for cryoprotection until the livers sank (approximately 12 h). Livers were then embedded in OCT freezing media and placed in -20°C for 12 h, and section of 14 μm were used for downstream applications.

#### *Pathological findings*

Kidney pathologies were examined according to Motamedi et al.[135] and Humphrey.[136] Initial pathology was assessed by presence of tubular lesions (nephrosis), were identified as small vacuoles that appeared in the tubular epithelium. Pathology progression was detected by cell swelling and extensive vacuolar degeneration of the tubular epithelium, in which the interstitium (lymphoid tissue) is infiltrated with lymphocytes. Liver pathologies were identified according to Humphrey,[136] Di Cicco et al.,[137] Feist et al.,[138] and Sternberg.[139] Initial pathology was assessed by liver fatty changes, including small droplets in hepatocytes. Pathology progression was detected as steatitis, in which hepatocytes are variable in size and some nuclei vary in size. Ovary pathologies were examined according to Motamedi et al.,[135] Di Cicco et al.[137] and Feist et al.[138] Briefly, atresia was considered as an increase in degradation and resorption of oocytes in development. Egg debris were detected by the presence of yolk within the oviduct.

#### *Staining of neutral lipid droplets*

Cryosections were stained for lipids droplets according to Griffett et al.[140] Briefly, slides were incubated in 2 μg/mL BODIPY 493/503 (Invitrogen™) in 1X DPBS for 15 min. Sections were washed three times in cold 1X DPBS and then counterstained with 1 μg/mL Hoechst. Three sections per liver, from a total of 3-4 fish, were imaged using the FV-1200 confocal microscope (Olympus, Japan). BODIPY intensity was normalized by nuclear staining,[141] quantified by ImageJ, and values were analyzed with GraphPad Prism.

### Dietary manipulations

#### *24 h fasting*

Following the morning feeding, fish were fasted for 24 h.

#### *Lifelong intermitted fasting*

Starting on week 4, fish were fed once a day for their remaining lifespan with a combination of GEMMA Micro 300 Fish Diet (Skretting Zebrafish, USA) supplemented by live Artemia.

#### *Short-term high-fat diet*

Old fish (15 weeks old) were fed twice a day, for a total of one week, with BioMar fish diet (0.5mm INICIO Plus SEA BREAM, BioMar Group, Demark), supplemented by live Artemia. This protocol was adapted from a recent report that demonstrated that killifish fed with BioMar INICIO had more visceral fat, and their livers possessed more lipid droplets.[142] As demonstrated for other short-term approaches in zebrafish,[143] one week of feeding with BioMar was sufficient for inducing significant accumulation of lipid droplets in the liver (when compared with our normal feeding, Figures 3F and S3F).

#### *Antibodies validation*

To validate antibody specificity using western blot, we generated two conditions in which AMPK-related pathways are expected to be altered. Specifically, male killifish were either starved for 3 days[79] or exposed to 20 mM 2-deoxy glucose for 2.5 h in system water (2-DG, Sigma Aldrich).[144] Specifically, in WT fish, we applied 3 days starvation or acute 2DG treatment (2-Deoxy-d-glucose, a glycolysis inhibitor) (Figure S5B). A canonical response was observed in the livers following acute 2DG treatment, while prolonged fasting mostly gave rise to metabolic adaptation.[145,146]

#### *17β-estradiol (E2) exposure*

17β-estradiol (E2, Holland Moran) was dissolved in ethanol, and sprayed on food pellets at 100 mg/kg for both drugs.[79] Food was then dried overnight under a chemical fume hood. Adult fish (9 weeks old) were individualized in tanks containing system water, and fed twice a day for a period of 8 days. Control groups were fed with ethanol treated food pellets and were similarly maintained and sampled. As expected, in response to the 17β-estradiol treatment, we observed lipid accumulation in treated fish.[147]

### Seahorse metabolic extracellular flux profiling

The Seahorse XFp Analyzer (Agilent Technologies, USA) was used to measure oxygen consumption rates (OCR, in pmol $O_2$ per min), and extracellular acidification rates (ECAR, in mpH per min). Primary fibroblasts from killifish tail fins were cultured as described above. The day before the experiment, cells were seeded (50,000 cells/well) in XFp 8-well plates (Agilent Technologies, USA). A relatively large number of cells was used in our assay to compensate for the small size and low basal respiration of primary fish cells. All the required drugs were supplied by the manufacturer (Seahorse Bioscience), and drug injection times were according to the XFp standard protocol. OCR and ECAR measurements were analyzed according to manufacturer's instructions and GraphPad Prism (v7, GraphPad).

Although cells were seeded in equal numbers to facilitate OCR and ECAR normalization, actual number of cells in each well was further confirmed using imaging to account for potential differences in proliferation rates. Briefly, following each metabolic assay, cells were fixed and stained for 15 min with 4% paraformaldehyde and 10 μM Hoechst 33342 (Thermo Fisher) in DPBS. Each well was imaged three times (IX83, Olympus), and averaged cell density (number of cells per field of view) was counted using CellProfiler (https://cellprofiler.org). Finally, the total number of cells per well was estimated by the relative area represented by the field of view, compared to the total area of the well. The following assays were performed 2-3 times. Each experiment contains at least three independent samples per genotype.

### Cell mito stress assay

Cell Mito Stress Test (XFp Cell Mito Stress Test Kit, Agilent Technologies) was performed following the manufacturers guidelines, with minor adaptations for fish cells described below. 1 h before the measurements, culture medium was replaced and the cells were incubated for 1 h min at 28°C with the Seahorse XF Base medium (Seahorse Bioscience), supplemented with 2 mM L-glutamine and 1 mM pyruvate (Seahorse Bioscience). Instead of glucose, we used 5 mM galactose (Sigma-Aldrich), which is the sugar source used by the L15 culture media. Oxygen consumption rate (OCR) and Extracellular Acidification Rate (ECAR) were detected after injection of oligomycin (1 μM), Carbonyl cyanide-p-trifluoromethoxyphenylhydrazone (FCCP, 1 μM), and the combination of rotenone & antimycin A (Rot/AA, 1 μM).

### Cell glycolysis stress assay

Cell Glycolysis Stress Test (XFp Glycolysis Stress Test Kit, Agilent Technologies) was performed following the standard protocol. Culture media was replaced by Seahorse XF Base medium, supplemented with 2 mM L-glutamine. During the test, final concentration of 15 mM glucose, 1 μM oligomycin, and 50 mM of 2-deoxyglucose (Seahorse Bioscience) were injected according to the XFp standard protocol.

### Proliferation of cultured cells

Cells from individual fish were seeded in 60 mm dish in triplicates, at a density of 200,000 cells/well. 24 h, 48 h, 72 h after seeding cells were counted using Neubauer counting chamber (MarienField #0640110). Medium was changed 4 h before the first counting point. Experiment was performed twice using 3 independent replicates per genotype (using the mean of three measurements per dish). Significance was calculated using two-way ANOVA and corrected by FDR.

## Pharmacological manipulation of cultured cells

### Adenine treatment

Cells were seeded in XFp 8-well plates (Agilent Technologies, USA) at a density of 50,000 cells/well and cultured overnight with adenine 10 μM. 1 h prior to the seahorse experiment, culture medium was replaced with the Seahorse XF Base medium (Agilent Technologies, USA) supplemented with adenine 10 μM (Sigma Aldrich), and cells were incubated for 1 h at 28°C.

### 8-azaadenine treatment

To characterize and validate the relative loss of APRT activity in heterozygous cells, an adenine analog, 8-azaadenine (Holland Moran) was used according to Jones and Sargent.[74] Briefly, mutant APRT cells that have reduced ability to metabolize adenine exhibit partial resistance to the toxic intermediate generated by AA.[74] Cells were treated with a range of concentrations of AA (0-200 μg/mL) for 4 days without media change. As AA is dissolved in 1 M NaOH, an equal amount of 1 M NaOH was added to the controls. Experiments were performed twice using 3 independent replicates per genotype.

### Serum starvation

Cells were seeded in a 12-well plate at a density of 100,000 cells/well. The following day, the medium was replaced with fresh media for 4 h, with L-15 medium containing either or 15% (control) or 5% FBS.

## Mitochondrial morphology

### Fluorescence microscopy

Cells were plated on a μ-Slide 8 Well Glass Bottom plates (ibidi, #80827), at a density of 40000 cells/well. Confocal imaging was performed on live cells using a sealed, environmentally controlled chamber without $CO_2$ at 28°C. A Day after, cells were labeled with 200 nM Mitoview 633 (Biotium) for 15 min prior to live imaging. Labeled cells were imaged on a laser scanning confocal microscope (FV-1200, Olympus, Japan) using a 60X/1.42 oil immersion objective. Scans were acquired using a sequential mode. All fluorophores were excited on separate tracks. Hoechst was excited with 405 nm and emission was captured through 485 nm short-pass filter. Mitoview 633 was excited with 561 nm and emission was captured through a 570-620 nm.

### Mitochondrial footprint and network analysis

To analyze mitochondrial morphology, we used MiNA (http://github.com/ScienceToolkit/MiNA), a plug-in macro toolset for Fiji.[148] This workflow estimates mitochondrial footprint from a binarized copy of the provided image, and the lengths of mitochondrial networks are estimated using a topological skeleton (mitochondrial length was defined as the length of rods and network branches). Additionally, we used the generated overlays (or a 3D rendering) to further confirm the accuracy of the analysis. Experiments were performed twice using 3 independent replicates per genotype. Three field of views, containing between 4-8 cells, were independently analyzed as described above.

## LC-MS for direct quantification of AMP, ADP, and ATP

Freshly seeded cells (in a T75 flask) were treated with control or Adenine containing media for 24h (as described above). Following treatment, cells reached 80% confluency (2-3 million cells/flask). Each sample was washed twice with chilled (4°C) phosphate buffered saline (PBS). 1.5 ml of extraction mix (standard Methanol/acetonitrile/water) was poured on each plate, and placed on a shaker at 4°C for 10 mins. The extraction solution was pipetted into a tube, and centrifuge 15 mins at max speed in 4°C. 1 ml of the supernatant was used for downstream analysis. For LC-MS, the Thermo Vanquish Flex ultra-high-performance liquid chromatography (UPLC) system coupled to Orbitrap Exploris 240 Mass Spectrometer (Thermo Fisher Scientific) was used. Resolution was set to 120,000 at 200 mass/charge ratio (m/z) with electrospray ionization and polarity switching mode to enable both positive and negative ions across a mass range of 67-1000 m/z. The chromatography was performed as described previously.[149] Briefly, UPLC setup

consisted ZIC-pHILIC column (SeQuant; 150 mm × 2.1 mm, 5 μm; Merck). 5 μl of cell extracts were injected and the compounds were separated using a mobile phase gradient of 15 min, starting at 20% aqueous (20 mM ammonium carbonate adjusted to pH 9.2 with 0.1% of 25% ammonium hydroxide): 80% organic (acetonitrile), and terminated with 20% acetonitrile. Flow rate and column temperature were maintained at 0.2 ml/min and 45°C, respectively, for a total run time of 27 min. All metabolites were detected using mass accuracy below 1 ppm. Thermo Xcalibur 4.4 was used for data acquisition. TraceFinder 4.1 was used for data analysis. Peak areas of metabolites were determined by using the exact mass of the single charged ions. The peak areas of different metabolites were determined using Thermo TraceFinder™ 4.1 software, where metabolites were identified by the exact mass of the single charged ion and by known retention time, using an in-house MS library built by running commercial standards of all detected metabolites. For data normalization, raw data files were processed with Compound Discoverer 3.1 to obtain total measurable ions peak intensities for each sample. Each identified metabolite intensity was normalized to the total intensity of the sample. Metabolite-Auto Plotter[150] was used for data visualization during data processing. Two samples were discarded from the analysis due to low quality (Table S4).

## Protein gel electrophoresis and immunoblotting

### *For liver samples*

Individual killifish, according to the specified age, gender, genotype, and feeding condition, were euthanized in 400 mg/L of Tricaine in system water. Animals were dissected on ice under a stereo microscope (Leica S9E) according to Astre et al.[44] All procedures were carried at 4°C unless stated otherwise. Homogenization was performed in a 2 mL Safe-Lock Tubes (Eppendorf), to allow full homogenization of liver tissue, using 3 mm-metal beads (Eldan Israel, Cat# RC55 420) and RIPA lysis buffer (7.9 g/L Tris-HCl, 9 g/L NaCl, 0.76 g/L EGTA, 10 ml 10% Triton X-100, pH 7.2). Prior to homogenization, 200 μl buffer was added to ~half a liver, and freshly supplemented with anti-protease and anti-phosphatase cocktail (Biotool). Homogenization was carried out with mechanical disruption using TissueLyzer LT (QIAGEN, #85600) with a dedicated adaptor (QIAGEN, #69980) at 50 Hz for 2 min X2. Protein concentration was measured with Pierce™ BCA Protein Assay Kit (Thermo Scientific™), according to manufacture instructions. 5-10 μg of liver homogenate was then mixed with the Sample Buffer (Tris-HCl pH 6.8 62.5 mM, Glycerol 10%, SDS 2%) at a ratio of 1:3. 2-mercaptoethanol (Sigma Aldrich) (5%) and Bromophenol blue (Sigma Aldrich) (0.02%) were freshly added, boiled at 95°C for 10 min, and placed on ice.

### *For primary culture*

Following a wash with cold DPBS, cells were re-suspended with 250 μl of the Sample Buffer (Tris-HCl pH 6.8 62.5 mM, Glycerol 10%, SDS 2%) at a ratio of 1:3, freshly supplemented with 5% 2-mercaptoethanol (Sigma Aldrich), 0.02% Bromophenol blue (Sigma Aldrich), and anti-protease and anti-phosphatase cocktail (Biotool). Samples were then boiled at 95°C for 10 min. 10 μl were used for western blot.

### *Immunoblotting*

Standard western blot was performed. Briefly, protein extracted (5-10 μg from livers, or 10 μl from cells) were resolved using Novex WedgeWell 4-20% Tris-Glycine gel (XP04205BOX, Thermo Fisher) and electrophoresed in Cell SureLock (Novex) in constant voltage of 50 V for 15 min (to clear stacking), followed by 120 V for 1 h. Transfer to a Nitrocellulose membrane was performed using the iBlot 2 (Thermo Scientific, IB21001), followed by Ponceau Red red staining (Sigma Aldrich, P7170-1L). Membranes were washed in TBST 0.1% (Tris-HCl 10mM pH 8.0, NaCl 150 mM, Tween 0.1%) once for 5 min to remove Ponceau staining, and blocked in 5% BSA (Sigma-Aldrich) in TBST for 1 h at room temperature. The resolved proteins were probed with the following antibodies at a concentration of 1:1000 (diluted in blocking solution at 4°C overnight): anti-AMPKα (CST-5831), anti-Phospho-AMPKα (Thr172) (CST-2535), anti-ACC (CST-3676), anti-Phospho-ACC (CST-3661), anti-S6 Ribosomal Protein (CST-2217), anti-Phospho-S6 Ribosomal Protein (CST-2211), and anti-Actin (MP Bio 0869100). Following three washes of 10min, membranes were incubated with 1:5000 HRP-conjugated goat anti-rabbit (ab6721, Abcam) or goat anti-mouse (ab6789, Abcam) antibodies for 1 h, and washed three times for 10 min. Chemiluminescence was detected using EZ-ECL kit (Biological Industry) and imaged with either ChemiDoc MP Imaging System (Biorad) or Fusion Pulse 6 (Vilbert Loumat). Band densitometry was quantified using ImageJ, and normalized according to Actin values.

## DNA isolation and measurement of mitochondrial DNA content using quantitative PCR

Quantification was performed according to Hartmann et al.[151] Briefly, total DNA from cells, tails and liver (age 15 weeks) was extracted using QIAamp Micro kit (Qiagen) according to the manufacturers protocol. The relative mitochondrial DNA (mtDNA) copy number was determined by quantitative PCR (qPCR) with the nuclear *CDKN2A/B* gene and the mitochondrial *16S rRNA* gene (primer sequences are available at Hartmann et al.[151]). qPCR was performed with Magnetic Induction Cycler (Mic, bio molecular systems) using Fast SYBR Green Master Mix (2X) (ThermoFisher 4385610), 100 nM of each primer, and 20 ng DNA as template. All reactions included negative controls (without template, or without the enzyme). Ct values of mtDNA were normalized to Ct values of the nuclear locus according to Hartmann et al.,[151] using the following equation: relative mtDNA copy number per diploid cell= $2\times2^{\Delta Ct}$, where ΔCt is $Ct_{CDKN2A/B\ locus}$-$Ct_{16S\ rRNA\ locus}$.

## A-to-I RNA editing

A-to-I editing is the most prevalent RNA editing. It is performed by double-stranded RNA-specific adenosine deaminase (ADAR) family of proteins.[152] Sequencing machines recognize Inosine as Guanosine, thus allowing us to quantify A-to-I editing by counting mismatches from Adenosine to Guanosine (A2G).[2]

### Quality control for RNA editing

Additional filtration steps, in addition to those performed for differential gene expression, were taken to eliminate common biases in RNA Editing. Specifically, we used PRINSEQ-lite 0.20.4[153] to remove exact duplicates, retain reads no shorter than 72 bp, and trim reads longer than 63 bp. Duplicate RNA reads, defined as reads with the same sequence on the same strand or with the reverse-compliment sequence on the opposite strand, can result from PCR cycles conducted before sequencing. Using only reads with similar lengths allowed us to compare the RNA Editing Index of different samples. Trimmomatic 0.39[154] was used to remove Nextera transposase adapters. Finally, we assessed the quality of the reads with FastQC 0.11.8[115] and MultiQC 1.11.[116]

### Genome and genomic annotations

Reads was mapped and quantified to the killifish genome Nfu_20140520.[41,119] As ADAR target editing sites are usually prevalent in repetitive regions,[152] we created a comprehensive annotation of these regions in the killifish genome by expanding the initial annotation. Specifically, we extracted the RepeatMaskerLib.embl library database using RepeatMasker 4.1.0,[155] and identified coding regions using the available GFF file. Finally, we used EDTA 1.9.6[156] to create an extended library of repeats.

### Signal-to-noise ratio (SNR)

Considering A-to-G editing as *Signal* and the 2$^{nd}$ most prevalent DNA-RNA mismatch other than A-to-G as *Noise*, we define SNR as:

$$SNR = \frac{Signal}{Signal + Noise} * 100$$

### Hyper editing and cluster screening

ADAR's activity is characterized by dense clusters of editing sites, which results in reads that are difficult to align by regular alignment procedures. Therefore, we applied an adaptation to successfully align those hyper-edited reads to the genome.[157] The output of this method is a list of hyper-edited sites and ultra-edited regions (UE). To get a clear SNR as possible, we applied a previously published approach,[158] termed here as Cluster Screening. Using a distance of 20 bp, we first required that two different editing sites (e.g., A2G and C2T) cannot reside within 20 bp next to each other. Second, each editing site must have a neighbor editing site of the same type, located no further than 20 bp from him. The first demand is meant to overcome alignment errors that are the result of duplication events. The second demand helps to identify clusters of editing sites, contrary to SNPs that occur randomly at various genomic locations. We dismissed editing sites that fail to satisfy either of these requirements.

### RNA editing index

To quantify the global editing levels of each UE cluster, we ran the RNA Editing Index tool.[159] For each kind of mismatch from *Reference Base* to *Mutated Base*, we define the Index of a region as

$$Index = \frac{Mutated\ Base}{Mutated\ Base + Reference\ Base} * 100$$

where *Reference Base* is the number of reads mapped to genomic positions (of that base), and *Mutated Base* is the number of reads with *Reference Base* to *Mutated Base* mismatch mapped to those positions. Specifically, the Index is a weighted average of RNA editing levels of a mismatch across a region. Using the Index allows us to compare RNA editing of different regions and samples. We ran the RNA Editing Indexer (https://github.com/a2iEditing/RNAEditingIndexer) with the following parameters as input: (1) The average expression level of each gene, as quantified by Salmon v1.4[160]; (2) RefSeq annotations of the genes and aligned BAM files. Independently of the Hyper Editing tool alignment, we aligned the Fastq files to the genome using BWA 0.7.17[161] with the MEM algorithm; (3) The UE clusters we previously chose with Cluster Screening. We ran the Index both in stranded and unstranded mode, but as the SNR of the stranded runs was lower, we decided to use its unstranded output. Independent t-tests were done using scipy.stats.ttest_ind 1.6.2, multiple independent t-tests were corrected using statsmodels.stats.multitest.fdrcorrection 0.12.2 using default parameters.

## QUANTIFICATION AND STATISTICAL ANALYSIS

### Statistics tests

The statistics tests of each panel are described on the legends. We used Shapiro test of normality in case we used parametric tests of small number size.